IEEE Access
Multidisciplinary | Rapid Review | Open Access Journal

Received February 9, 2022, accepted March 3, 2022, date of publication March 8, 2022, date of current version March 15, 2022.

Digital Object Identifier 10.1109/ACCESS.2022.3157326

Design of Static Output Feedback Controllers for an Active Suspension System

YONGHWAN JEONG[1], YOUNGIL SOHN[2], SEHYUN CHANG[2], AND SEONGJIN YIM[1], (Member, IEEE)

[1]Department of Mechanical and Automotive Engineering, Seoul National University of Science and Technology, Nowon-gu, Seoul 01811, Republic of Korea
[2]Institute of Advanced Technology Development, Hyundai Motor Company, Seongnam-si, Gyeonggi-do 13529, Republic of Korea

Corresponding author: Seongjin Yim (acebtif@seoultech.ac.kr)

This work was supported by the Research Program funded by Hyundai Motor Group.

ABSTRACT This paper presents a method by which to design linear quadratic (LQ) static output feedback (SOF) controllers with a 2-DOF quarter-car model for an active suspension system. Generally, it is challenging to implement linear quadratic regulator (LQR), designed with a full-car model, in actual vehicles because doing so requires 14 state variables to be precisely measured. For this reason, LQR has been designed with a quarter-car model and then applied to a full-car model. Although this requires far fewer state variables, some of them are still difficult to measure. Thus, it is necessary to design a LQ SOF controller which uses available sensor signals that are relatively easily measured in real vehicles. In this paper, a LQ SOF controller is designed with a quarter-car model and applied to a full-car model for ride comfort. To design the controller, an optimization problem is formulated and solved by a heuristic optimization method. A frequency domain analysis and a simulation with a simulation package show that the proposed LQ SOF controllers effectively improve the ride comfort with an active suspension system.

INDEX TERMS Active suspension control, static output feedback control, 2-DOF quarter-car model, 7-DOF full-car model, linear quadratic regulator.

I. INTRODUCTION

Generally, it is known that there are two objectives when designing a suspension system of an actual vehicle: ride comfort and road adhesion. There are also typical three measures or performance indices when evaluating these objectives: vertical acceleration, the suspension stroke and tire deflection [1]. Ride comfort is evaluated with vertical acceleration and the roll and pitch angles of the sprung mass of the vehicle. According to ISO2631-1, pertaining to the sensitivity of the human body to vibrations, it is necessary to reduce vertical acceleration at frequencies within the range of 4 to 10Hz, and to do the roll and pitch angles of the sprung mass at frequencies within the range of 0.5 to 2Hz for the purpose of improving the ride comfort [2], [3]. Road adhesion or road holding is evaluated by assessing the suspension stroke and tire deflection. The smaller the suspension stroke and the larger the tire deflection are, the better the road adhesion becomes. Generally, it is known that there is trade-off between ride comfort and road adhesion [1], [4], [5]. For example, the suspension stroke increases and the tire deflection decreases smaller if the suspension is softly tuned. As a result, the ride comfort is improved and road adhesion deteriorates [4].

The active suspension system can improve ride comfort by reducing the road-induced vertical acceleration of the sprung mass with a number of actuators. In other words, the role of an active suspension system is to attenuate the effect of the road profile or the road-induced vibration on the sprung mass by means of some actuators. In relations to this, an active suspension controller can be used for disturbance attenuation or vibration isolation. To date, numerous papers on the design of controllers for active suspension systems have been published [6]–[21]. In view of the dynamic models used for controller design purpose, the 2-DOF quarter-car, 4-DOF half-car, and 7-DOF full-car models have been used. Among them, the 2-DOF quarter-car model is most frequently used [4], [6]–[17]. With regard to controller design methodologies, the linear optimal control, nonlinear control, and adaptive control theories have been adopted. Since 2010, H_∞ control has been the most widely used methodology for suspension control [7], [8], [13]–[15], [19]. Regarding the

The associate editor coordinating the review of this manuscript and approving it for publication was Ton Duc Do.

actuators used to generate active force, hydraulic actuators and electric motors have been applied [9], [10], [14], [15], [17], [19], [21]. Comprehensive surveys of active suspension control methods, including those related to dynamic models, controller designs, and actuators, can be found in the literature [1], [4], [22]–[26].

Among several controller design methodologies proposed for active suspension control, the linear quadratic regulator (LQR) has been adopted because it can provide a systematic way to design a full-state feedback controller for active suspension by tuning the weights of performance measures such as the ride comfort and road adhesion [1], [4], [27]. The LQR has been designed with state-space equations derived from the 2-DOF quarter-car, 4-DOF half-car and 7-DOF full-car models. As mentioned earlier, the most frequently used model in designs of a controller for an active suspension system is the 2-DOF quarter-car model. On the other hand, the 7-DOF full-car model is most relevant to actual vehicles because it describes the vertical, roll and pitch motions of a single sprung mass and the vertical motions of four unsprung masses [23]. However, a controller designed with the quarter-car model has not been applied to the full-car case except in one study [27]. An active suspension controller has also been designed with the full-car model in case the designed controller is to be applied to actual vehicles [20], [21], [27].

If 2-DOF quarter-car, 4-DOF half-car and 7-DOF full-car models are used to design a LQR for an active suspension system, four, eight and fourteen state variables, respectively, must be precisely measured for full-state feedback control. However, most state variables in these models cannot be measured or are difficult to measure using sensors in real vehicles. To cope with this problem, a state observer or estimator has been designed with these models. Generally, a Kalman filter has been adopted as a state observer for a full-state feedback controller or LQR. To date for active suspension control, the combination of Kalman filter and a LQR, i.e., the linear quadratic Gaussian (LQG), has been studied extensively [27]–[30].

Generally, it is not easy to implement a LQR designed with the full-car model for active suspension control in an actual vehicle given the numerous state variables and control inputs. For example, there are one, two, and four control inputs for the quarter-car, half-car and full-car models, respectively. Therefore, the dimensions of the gain matrices of LQRs for the quarter-car, half-car and full-car models are 1×4, 2×8 and 4×14, respectively. For this reason, it is challenging to implement a LQR designed with the full-car model on actual vehicles or in vehicle simulation packages such as CarSim or CarMaker. Accordingly, it is necessary to design a controller with a simpler structure that requires fewer elements in the gain matrix.

In this paper, 2-DOF quarter-car and 7-DOF full-car models are adopted in the design of a controller for an active suspension system. A LQR is designed with the quarter-car model instead of the full-car case because there are far fewer state variables and control inputs in the quarter-car model than in the full-car model. To avoid measuring the state variables for the LQR, the LQ SOF controller is designed with available sensor signals [31], [32]. Generally, there are far fewer available sensor signals used for LQ SOF controllers than those for state variables for the LQR. Therefore, it is much easier to implement a LQ SOF controller in an actual vehicle compared to a LQR. To find the gain matrix of the LQ SOF controller, an optimization problem is formulated. Because there are no guaranteed methods by which to find a stabilizing or optimal controller for LQ SOF control, a heuristic optimization method is applied to find an optimal gain matrix in this case. Then, the LQ SOF controller designed with the quarter-car model is directly applied to the full-car model consider the fact that each corner of the full-car model can be regarded as the quarter model [27]. It can be expected that this controller has little effects on the roll and pitch angles of the sprung mass because it cannot use the roll and pitch angles or the rates for feedback due to the quarter-car model. To cope with this problem, the LQ SOF controller is designed with the full-car model and extra sensor signals, i.e., roll and pitch rates for feedback. Instead of using extra sensor signals for feedback, the terms related to the roll and pitch angles or rates can be added into LQ objective functions. To assess the effectiveness of the proposed controllers for active suspension control, a frequency-domain analysis and a simulation with the vehicle simulation package CarMaker are conducted. The designed LQ SOF controllers are compared through the analysis and simulation in terms of the ride comfort.

The main contributions of this paper are summarized below:

1) For active suspension control, LQ SOF controllers with far fewer gain elements are designed with the quarter-car model and applied to the full-car model.
2) To find the optimum gain matrices of the LQ SOF controllers, an optimization problem is formulated and solved by a heuristic optimization method.
3) To improve the control performance for roll and pitch motions of the sprung mass, LQ SOF controllers are designed with roll and pitch rate signals given in the full-car model.

This paper consists of four sections. In Section II, state-space equations are derived from 2-DOF quarter-car and 7-DOF full-car models. Based on these models, the LQR and LQ SOF controllers for active suspension are designed. In Section III, frequency-domain analyses and simulations with a vehicle simulation package for the designed controllers are conducted. The conclusions are given in Section IV.

II. CONTROLLER DESIGN FOR ACTIVE SUSPENSION

A. LQR DESIGN WITH A QUARTER-CAR MODEL

Fig. 1 shows a 2-DOF quarter-car model. This model describes the vertical motions of the sprung and unsprung masses, m_s and m_u, respectively. The dynamic variables are z_s

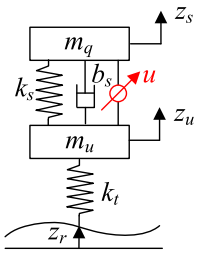

FIGURE 1. 2-DOF quarter-car model.

and z_u, which are correspondingly the vertical displacements of the sprung and unsprung masses. The control input or active force u generated by an actuator is located between the sprung and unsprung masses. The disturbance is the road profile, z_r.

With the suspension stroke and its rate, the suspension force f between the sprung and unsprung masses is calculated as (1). With the suspension force f, the equations of motion of the sprung and unsprung masses are derived as (2). The vector of state variables of the quarter-car model is defined as (3). With these definitions, the state-space equation for the quarter-car model is derived as (4). The detailed procedure of the derivation on the matrices $\mathbf{A}_q$, $\mathbf{B}_{1q}$ and $\mathbf{B}_{2q}$ can be found in the literature [27].

$$f = -k_s(z_s - z_u) - b_s(\dot{z}_s - \dot{z}_u) + u \tag{1}$$

$$\begin{cases} m_q \ddot{z}_s = f \\ m_u \ddot{z}_u = -f - k_t(z_u - z_r) \end{cases} \tag{2}$$

$$\mathbf{x}_q = \begin{bmatrix} z_s & z_u & \dot{z}_s & \dot{z}_u \end{bmatrix}^T \tag{3}$$

$$\dot{\mathbf{x}}_q = \mathbf{A}_q \mathbf{x}_q + \mathbf{B}_{1q} z_r + \mathbf{B}_{2q} u \tag{4}$$

With the state variables in the quarter-car model, the LQ objective function for the active suspension system is defined as (5). The weight ρ_i emphasizes the corresponding term in (5). Several methods have been proposed for determining these weights [33]–[37]. In this paper, Bryson's rule (6) is adopted to select the weights [33]. In (6), η is the maximum allowable value for the corresponding term. For ride comfort, the value of η_1 for the vertical acceleration of the sprung mass should be set to a lower value while holding the other values of η_i constant. On the other hand, for road adhesion or cornering, the values of η_2 and η_3, respectively, on the suspension stroke and tire deflection should be higher. From (5), the weighting matrices are derived as $\mathbf{Q}_q$, $\mathbf{N}_q$ and $\mathbf{R}_q$. LQR is a controller with the form of full-state feedback, (7), which minimizes J_q. The controller gain matrix $\mathbf{K}_q$ is calculated from Riccati equation with $\mathbf{A}_q$, $\mathbf{B}_{2q}$, $\mathbf{Q}_q$, $\mathbf{N}_q$ and $\mathbf{R}_q$. As shown in (7), there are four elements in the gain matrix identical to the number of state variables, as given in (3). We denote this controller $\mathbf{K}_q$ as LQRq.

$$J_q = \int_0^\infty \left\{ \rho_1 \ddot{z}_s^2 + \rho_2 (z_s - z_u)^2 + \rho_3 z_u^2 + \rho_4 u^2 \right\} dt$$

$$= \int_0^\infty \left\{ \begin{bmatrix} \mathbf{x}_q \\ u \end{bmatrix}^T \begin{bmatrix} \mathbf{Q}_q & \mathbf{N}_q \\ \mathbf{N}_q^T & \mathbf{R}_q \end{bmatrix} \begin{bmatrix} \mathbf{x}_q \\ u \end{bmatrix} \right\} dt \tag{5}$$

$$\rho_i = 1/\eta_i^2, \quad i = 1, 2, 3, 4 \tag{6}$$

$$u_q = -\mathbf{K}_q \mathbf{x}_q = -\begin{bmatrix} k_1 & k_2 & k_3 & k_4 \end{bmatrix} \mathbf{x}_q \tag{7}$$

B. LQR DESIGN WITH A FULL-CAR MODEL

Fig. 2 shows a 7-DOF full-car model, which describes the vertical, roll and pitch motions of the sprung mass, and the vertical motions of four unsprung masses. As shown in Fig. 2, the front left, front right, rear left and rear right corners are numbered as ①, ②, ③ and ④, respectively. Dynamic variables in the model are z_c, φ, θ, z_{u1}, z_{u2}, z_{u3}, z_{u4}, where the first three are the vertical displacement, the roll angle and the pitch angle of the sprung mass, and the last four are the vertical displacements of the unsprung masses, respectively. In the model, the road profiles, z_{r1}, z_{r2}, z_{r3} and z_{r4}, are four external disturbances acting on the unsprung mass. The control inputs, u_1, u_2, u_3 and u_4, at each suspension are generated by an actuator located between the sprung and unsprung masses.

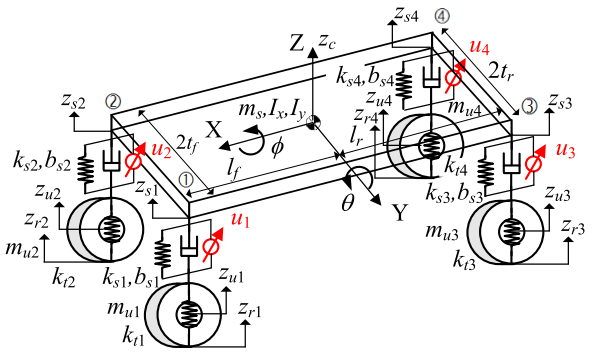

FIGURE 2. 7-DOF full-car model.

As given in (1), the suspension forces in the full-car model are derived as (8). In (8), u_i is the control input or active force applied to the i-th suspension. With the definitions of the suspension forces, the equations of motions for the sprung and unsprung masses are given in (9) and (10), respectively. The equations of motion of the sprung mass, (9), can be represented as the vector-matrix form, (11). In (11), the matrix G represents the geometric relationship between the forces and moments acting on the sprung mass and the suspension forces.

$$f_i = -k_{si}(z_{si} - z_{ui}) - b_{si}(\dot{z}_{si} - \dot{z}_{ui}) + u_i, \quad i = 1, 2, 3, 4 \tag{8}$$

$$\begin{cases} m_s \ddot{z}_c = f_1 + f_2 + f_3 + f_4 \\ I_x \ddot{\phi} = t_f \cdot f_1 - t_f \cdot f_2 + t_r \cdot f_3 - t_r \cdot f_4 \\ I_y \ddot{\theta} = -l_f \cdot (f_1 + f_2) + l_r \cdot (f_3 + f_4) \end{cases} \tag{9}$$

$$m_{ui} \ddot{z}_{ui} = -f_i + k_{ti}(z_{ui} - z_{ri}), \quad i = 1, 2, 3, 4 \tag{10}$$

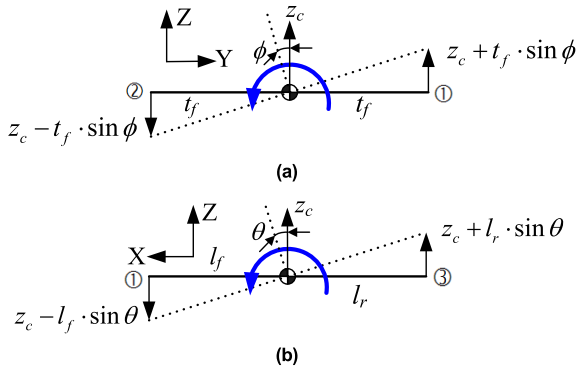

FIGURE 3. Roll and pitch motions of the sprung mass. (a) Roll motion (b) Pitch motion.

$$\begin{bmatrix} m_s\ddot{z}_c \\ I_x\ddot{\phi} \\ I_y\ddot{\theta} \end{bmatrix} = \underbrace{\begin{bmatrix} 1 & 1 & 1 & 1 \\ t_f & -t_f & t_r & -t_r \\ -l_f & -l_f & l_r & l_r \end{bmatrix}}_{\mathbf{G}} \begin{bmatrix} f_1 \\ f_2 \\ f_3 \\ f_4 \end{bmatrix} = \mathbf{G} \begin{bmatrix} f_1 \\ f_2 \\ f_3 \\ f_4 \end{bmatrix} \tag{11}$$

Fig. 3 shows the roll and pitch motions of the sprung mass. From the geometry given in Fig. 3, the vertical displacements of the sprung mass, i.e., z_{s1}, z_{s2}, z_{s3} and z_{s4}, at each corner are calculated as (12) in a geometrical manner under the assumption that the sprung mass is a rigid body. Under the condition that the absolute values of the roll and pitch angles are less than 10 deg, the sine functions in (12) are linearized as $\sin\theta \simeq \theta$ and $\sin\phi \simeq \phi$. As a result, (12) can be converted to the vector-matrix form of (13). In (13), the matrix $\mathbf{G}$ is identical to that of (11), which represents the geometrical relationship between the vertical displacements and the roll and pitch angles of the sprung mass.

$$\begin{cases} z_{s1} = z_c + t_f \cdot \sin\phi - l_f \cdot \sin\theta \\ z_{s2} = z_c - t_f \cdot \sin\phi - l_f \cdot \sin\theta \\ z_{s3} = z_c + t_f \cdot \sin\phi + l_r \cdot \sin\theta \\ z_{s4} = z_c - t_f \cdot \sin\phi + l_r \cdot \sin\theta \end{cases} \tag{12}$$

$$\begin{bmatrix} z_{s1} \\ z_{s2} \\ z_{s3} \\ z_{s4} \end{bmatrix} = \underbrace{\begin{bmatrix} 1 & t_f & -l_f \\ 1 & -t_f & -l_f \\ 1 & t_r & l_r \\ 1 & -t_r & l_r \end{bmatrix}}_{\mathbf{G}^T} \begin{bmatrix} z_c \\ \phi \\ \theta \end{bmatrix} = \mathbf{G}^T \begin{bmatrix} z_c \\ \phi \\ \theta \end{bmatrix} \tag{13}$$

The vectors of state variables, disturbances and control inputs are defined as (14). With these definitions, (13) is represented as (15). The vector of state variables for the full-car model is defined as (16). With this definition, the state-space equation for the 7-DOF full-car model is obtained as (17). (4). The detailed procedure by which of the matrices $\mathbf{A}_f$, $\mathbf{B}_{1f}$ and $\mathbf{B}_{2f}$ are derived can be found in the earlier study [27].

$$\begin{cases} \mathbf{z}_s \triangleq \begin{bmatrix} z_{s1} & z_{s2} & z_{s3} & z_{s4} \end{bmatrix}^T, \\ \mathbf{z}_u \triangleq \begin{bmatrix} z_{u1} & z_{u2} & z_{u3} & z_{u4} \end{bmatrix}^T \\ \mathbf{z}_r \triangleq \begin{bmatrix} z_{r1} & z_{r2} & z_{r3} & z_{r4} \end{bmatrix}^T \\ \mathbf{p} \triangleq \begin{bmatrix} z_c & \phi & \theta \end{bmatrix}^T, \ \mathbf{q} \triangleq \begin{bmatrix} \mathbf{p} \\ \mathbf{z}_u \end{bmatrix}, \\ \mathbf{u}_f \triangleq \begin{bmatrix} u_1 & u_2 & u_3 & u_4 \end{bmatrix}^T, \ \mathbf{w}_f = \mathbf{z}_r \end{cases} \tag{14}$$

$$\mathbf{z}_s = \mathbf{G}^T \mathbf{p} \tag{15}$$

$$\mathbf{x}_f \triangleq \begin{bmatrix} \mathbf{q} \\ \dot{\mathbf{q}} \end{bmatrix} \tag{16}$$

$$\dot{\mathbf{x}}_f = \mathbf{A}_f \mathbf{x}_f + \mathbf{B}_{1f} \ \mathbf{w}_f + \mathbf{B}_{2f} \mathbf{u}_f \tag{17}$$

With the state variables in the full-car model, the LQ objective function for active suspension control is defined as (18). This LQ objective function is quite general in that it has all of the terms regarding ride comfort and road adhesion. According to Bryson's rule, the weights of (18) are set to $\rho_i = 1/\eta_i^2$, as given in (5). For ride comfort, the weights ρ_1, ρ_7, and ρ_9 on the vertical, roll and pitch angles should be set to higher values while holding the other values constant. In contrast, for road adhesion, the weights ρ_2 and ρ_3 on the suspension stroke and the tire deflection should be set to higher values while holding the other values constant. As shown in (18), the first four terms are identical to those of (5). Therefore, the LQR for the full-car model can be designed such that it has performance equivalent to that of the quarter-car model. The LQR for the full-car model is a controller with the form of full-state feedback, (19), which minimizes J_f. The controller gain matrix $\mathbf{K}_f$ is calculated from the Riccati equation with $\mathbf{A}_f$, $\mathbf{B}_{2f}$, $\mathbf{Q}_f$, $\mathbf{N}_f$ and $\mathbf{R}_f$. Here, we denote this controller $\mathbf{K}_f$ as LQRf1.

$$J_f = \int_0^\infty \left\{ \begin{array}{l} \rho_1 \ddot{z}_c^2 + \rho_2 \sum_{i=1}^4 (z_{si} - z_{ui})^2 + \rho_3 \sum_{i=1}^4 z_{ui}^2 \\ +\rho_4 \sum_{i=1}^4 u_i^2 + \rho_5 \ddot{\phi}^2 + \rho_6 \ddot{\theta}^2 + \rho_7 \phi^2 + \rho_8 \dot{\phi}^2 \\ +\rho_9 \theta^2 + \rho_{10} \dot{\theta}^2 \end{array} \right\} dt$$

$$= \int_0^\infty \left\{ \begin{bmatrix} \mathbf{x}_f \\ \mathbf{u}_f \end{bmatrix}^T \begin{bmatrix} \mathbf{Q}_f & \mathbf{N}_f \\ \mathbf{N}_f^T & \mathbf{R}_f \end{bmatrix} \begin{bmatrix} \mathbf{x}_f \\ \mathbf{u}_f \end{bmatrix} \right\} dt \tag{18}$$

$$u_f = -\mathbf{K}_f \mathbf{x}_f = -\mathbf{K}_f \begin{bmatrix} \mathbf{q} \\ \dot{\mathbf{q}} \end{bmatrix} \tag{19}$$

As mentioned earlier, the LQ objective function, (18), becomes (20) by setting $\rho_5 \sim \rho_{10}$ to zero. This function has a form identical to that of (5). The controller gain matrix $\mathbf{K}_f$ in (19) is calculated from the Riccati equation with $\mathbf{A}_f$, $\mathbf{B}_{2f}$,

$\mathbf{Q}_{fq}$, $\mathbf{N}_{fq}$ and $\mathbf{R}_{fq}$. We denote this controller as LQRf2.

$$J_{fq} = \int_0^\infty \left\{ \begin{array}{l} \rho_1 \sum_{i=1}^{4} \ddot{z}_{si}^2 + \rho_2 \sum_{i=1}^{4} (z_{si} - z_{ui})^2 \\ +\rho_3 \sum_{i=1}^{4} z_{ui}^2 + \rho_4 \sum_{i=1}^{4} u_i^2 \end{array} \right\} dt$$
$$= \int_0^\infty \left\{ \begin{bmatrix} \mathbf{x}_f \\ \mathbf{u}_f \end{bmatrix}^T \begin{bmatrix} \mathbf{Q}_{fq} & \mathbf{N}_{fq} \\ \mathbf{N}_{fq}^T & \mathbf{R}_{fq} \end{bmatrix} \begin{bmatrix} \mathbf{x}_f \\ \mathbf{u}_f \end{bmatrix} \right\} dt \quad (20)$$

In (20), there are no terms on the roll and pitch angles. Accordingly, to emphasize the roll and pitch angles of the sprung mass, the LQ objective function (20) is modified into (21) by setting ρ_5, ρ_6, ρ_8 and ρ_{10} in (18) to zero. The controller gain matrix $\mathbf{K}_f$ is calculated from the Riccati equation with $\mathbf{A}_f$, $\mathbf{B}_{2f}$, $\mathbf{Q}_{fr}$, $\mathbf{N}_{fr}$ and $\mathbf{R}_{fr}$. We denote this controller as LQRf3.

$$J_{fr} = \int_0^\infty \left\{ \begin{array}{l} \rho_1 \ddot{z}_c^2 + \rho_2 \sum_{i=1}^{4} (z_{si} - z_{ui})^2 + \rho_3 \sum_{i=1}^{4} z_{ui}^2 \\ +\rho_4 \sum_{i=1}^{4} u_i^2 + \rho_7 \phi^2 + \rho_9 \theta^2 \end{array} \right\} dt$$
$$= \int_0^\infty \left\{ \begin{bmatrix} \mathbf{x}_f \\ \mathbf{u}_f \end{bmatrix}^T \begin{bmatrix} \mathbf{Q}_{fr} & \mathbf{N}_{fr} \\ \mathbf{N}_{fr}^T & \mathbf{R}_{fr} \end{bmatrix} \begin{bmatrix} \mathbf{x}_f \\ \mathbf{u}_f \end{bmatrix} \right\} dt \quad (21)$$

The LQR provides a systematic way to design an active suspension controller. LQRf1, LQRf2 and LQRf3 are full-state feedback controllers with identical control structures, (19), and different LQ objective functions, (18), (20) and (21), respectively. As shown in (14), (16) and (19), there are fourteen and four state variables and control inputs for the full-car model, respectively. Therefore, the dimension of the gain matrix $\mathbf{K}_f$ of the LQR is 4×14, which is too complex to be implemented in an actual vehicle. Moreover, to implement the controller in an existing vehicle, it is necessary to measure or estimate all state variables in $\mathbf{x}_f$ precisely. However, it is difficult to measure those variables by sensors in real vehicles. For this reason, it is necessary to design a controller which requires fewer state variables and that uses available sensor signals so as to implement the controller in an actual vehicle more feasibly.

C. LQ SOF CONTROLLER DESIGN WITH THE QUARTER-CAR MODEL

When implementing the LQR designed with the quarter-car model in an actual vehicle, it is difficult to measure the state variables of (3). For example, it is not easy to measure the vertical displacements of the sprung and unsprung masses and the suspension stroke if using a sensor. To cope with this problem, SOF is adopted. SOF uses available sensor signals for feedback control [38], [39]. SOF has been adopted for active suspension control [40], [41]. For the quarter-car model, the typical available sensor signals are the vertical acceleration of the sprung mass and the suspension stroke. These signals have been used for semi-active suspension control [42]–[46]. The suspension stroke is measured by displacement sensors such as the laser displacement type or with a linear variable differential transformer (LVDT) [43]. The suspension stroke rate can be obtained by differentiating the suspension stroke with a filter [44]. For the full-car model, the roll and pitch rates of the sprung mass can easily be measured by an inertial measurement unit (IMU). Thus, it is assumed that the vertical acceleration and the roll and pitch angles of the sprung mass and the suspension stroke and the corresponding rate can be measured by sensors and can be made available for feedback control. In the quarter-car model, the vertical acceleration, the suspension stroke and the corresponding rate are available for feedback control.

The SOF controller has the form of (22). Because there are three sensor measurements available for feedback control, three output matrices can be defined as $\mathbf{y}_{q1}$, $\mathbf{y}_{q2}$ and $\mathbf{y}_{q3}$ as given in (23), (24), and (25) from the definitions of the state vector (3) and the state-space equation (4). In (23) and (24), $\mathbf{A}_{q,3}$ and $\mathbf{B}_{2q,3}$ represent the third rows of the matrices $\mathbf{A}_q$ and $\mathbf{B}_{2q}$, respectively. As shown in (23), (24), and (25), the sensor outputs have two elements. Therefore, there are also two elements in the gain matrix, $\mathbf{K}_{SOF}$, while $\mathbf{K}_q$ of the LQR has four elements. By replacing $\mathbf{y}_q$ in (22) with $\mathbf{y}_{q1}$, $\mathbf{y}_{q2}$ and $\mathbf{y}_{q3}$, the control inputs u_{q1}, u_{q2} and u_{q3} are obtained as (26). After some algebraic manipulation, the control inputs u_{q1}, u_{q2} and u_{q3} are obtained as the full-state feedback form of (27). From (27), the full-state feedback gain matrices of u_{q1}, u_{q2} and u_{q3}, i.e., $\mathbf{V}_{q1}$, $\mathbf{V}_{q2}$ and $\mathbf{V}_{q3}$, are obtained as (28).

$$u = \mathbf{K}_{SOF}\mathbf{y}_q \quad (22)$$

$$\mathbf{y}_{q1} = \begin{bmatrix} \ddot{z}_s \\ z_s - z_u \end{bmatrix} = \begin{bmatrix} \mathbf{A}_{q,3} \\ 1 \quad -1 \quad 0 \quad 0 \end{bmatrix} \mathbf{x}_q + \begin{bmatrix} \mathbf{B}_{2q,3} \\ 0 \end{bmatrix} u$$
$$= \mathbf{C}_{s1}\mathbf{x}_q + \mathbf{D}_s u \quad (23)$$

$$\mathbf{y}_{q2} = \begin{bmatrix} \ddot{z}_s \\ \dot{z}_s - \dot{z}_u \end{bmatrix} = \begin{bmatrix} \mathbf{A}_{q,3} \\ 0 \quad 0 \quad 1 \quad -1 \end{bmatrix} \mathbf{x}_q + \begin{bmatrix} \mathbf{B}_{2q,3} \\ 0 \end{bmatrix} u$$
$$= \mathbf{C}_{s2}\mathbf{x}_q + \mathbf{D}_s u \quad (24)$$

$$\mathbf{y}_{q3} = \begin{bmatrix} z_s - z_u \\ \dot{z}_s - \dot{z}_u \end{bmatrix} = \begin{bmatrix} 1 & -1 & 0 & 0 \\ 0 & 0 & 1 & -1 \end{bmatrix} \mathbf{x}_q = \mathbf{C}_{s3}\mathbf{x}_q \quad (25)$$

$$\left\{ \begin{array}{l} u_{q1} = \mathbf{K}_{SOF1}\mathbf{y}_{q1} = \mathbf{K}_{SOF1}\mathbf{C}_{s1}\mathbf{x}_q + \mathbf{K}_{SOF1}\mathbf{D}_s u_{q1} \\ u_{q2} = \mathbf{K}_{SOF2}\mathbf{y}_{q2} = \mathbf{K}_{SOF2}\mathbf{C}_{s2}\mathbf{x}_q + \mathbf{K}_{SOF2}\mathbf{D}_s u_{q2} \\ u_{q3} = \mathbf{K}_{SOF3}\mathbf{y}_{q3} = \mathbf{K}_{SOF3}\mathbf{C}_{s3}\mathbf{x}_q \end{array} \right. \quad (26)$$

$$\left\{ \begin{array}{l} u_{q1} = (\mathbf{I} - \mathbf{K}_{SOF1}\mathbf{D}_s)^{-1}\mathbf{K}_{SOF1}\mathbf{C}_{s1}\mathbf{x}_q = \mathbf{V}_{q1}\mathbf{x}_q \\ u_{q2} = (\mathbf{I} - \mathbf{K}_{SOF2}\mathbf{D}_s)^{-1}\mathbf{K}_{SOF2}\mathbf{C}_{s2}\mathbf{x}_q = \mathbf{V}_{q2}\mathbf{x}_q \\ u_{q3} = \mathbf{K}_{SOF3}\mathbf{C}_{s3}\mathbf{x}_q = \mathbf{V}_{q3}\,\mathbf{x}_q \end{array} \right. \quad (27)$$

$$\left\{ \begin{array}{l} \mathbf{V}_{q1} \triangleq (\mathbf{I} - \mathbf{K}_{SOF1}\mathbf{D}_s)^{-1}\mathbf{K}_{SOF1}\mathbf{C}_{s1} \\ \mathbf{V}_{q2} \triangleq (\mathbf{I} - \mathbf{K}_{SOF2}\mathbf{D}_s)^{-1}\mathbf{K}_{SOF2}\mathbf{C}_{s2} \\ \mathbf{V}_{q3} \triangleq \mathbf{K}_{SOF3}\mathbf{C}_{s3} \end{array} \right. \quad (28)$$

With the full-state feedback form of (27) and (28), the LQ SOF controller design problem is formulated as an optimization problem, as given in (29). The optimization problem is to find $\mathbf{K}_{SOF}$ which minimizes the LQ objective function J_q. In (29), two elements of $\mathbf{K}_{SOF}$ are the optimization variables. If two elements are assumed to have arbitrary values, then the SOF controller gain $\mathbf{K}_{SOF}$ and its corresponding full-state feedback controller gain $\mathbf{V}_q$ are obtained as (28). For stable $\mathbf{V}_q$, the solution $\mathbf{P}_q$ of the Lyapunov equation in (29) is obtained. The value of the LQ objective function J_q is calculated as trace($\mathbf{P}_q$). It is known that there are no methods that guarantee the finding of a global optimum or stable initial solution for LQ SOF control because the optimization problem is non-convex and the controller gain matrix $\mathbf{V}_q$ is structured [38], [39].

$$\min_{\mathbf{K}_{SOF}} J_q = \frac{1}{2}\text{trace}\left(\mathbf{P}_q\right)$$
$$s.t. \begin{cases} \mathbf{P}_q = \mathbf{P}_q^T > \mathbf{0} \\ \max\left(Re\left[\mathbf{A}_q + \mathbf{B}_{2q}\mathbf{V}_q\right]\right) < 0 \\ \left(\mathbf{A}_q + \mathbf{B}_{2q}\mathbf{V}_q\right)^T \mathbf{P}_q + \mathbf{P}_q\left(\mathbf{A}_q + \mathbf{B}_{2q}\mathbf{V}_q\right) \\ +\mathbf{Q}_q + \mathbf{V}_q^T\mathbf{N}_q^T + \mathbf{N}_q\mathbf{V}_q + \mathbf{V}_q^T\mathbf{R}_q\,\mathbf{V}_q = \mathbf{0} \end{cases} \quad (29)$$

Generally, to solve non-convex and non-linear optimization problems, heuristic optimization methods such as genetic algorithm (GA), the evolutionary strategy (ES) and particle swarm optimization (PSO) have been proposed [47], [48]. Most heuristic optimization methods have the procedure of initialization, evaluation, selection and reproduction, as given in Fig. 4. Different from gradient-based search methods, heuristic optimization methods have multiple solutions. The group of these solutions is called a population, which is denoted as $\mathbf{P}(k)$ in Fig. 4. In heuristic optimization methods, the iteration is referred to with the term generation. In Fig. 4, k is the iteration or generation index. After generating random initial solutions, the objective function is evaluated for each solution in the population. Based on the objective function values, some of solutions are selected for use in the next generation. Selection is done in such a way that better solutions will survive through generation. New solutions are generated by reproduction. Typical reproduction operators are crossover and mutation in the GA. This procedure is iterated by a predetermined number. Because heuristic optimization methods have multiple solutions, it is easy to escape from local optima although a global optimum cannot be guaranteed. To have the search direction move to a wider or narrower feasible region, reproduction operators are used. For the reasons, it is known that heuristic optimization methods are quite effective when used to solve non-convex and non-linear optimization problems.

In this paper, to find the optimum gain $\mathbf{K}_{SOF}$, the heuristic optimization method, CMA-ES, is applied [49]. CMA-ES, an evolutionary strategy with a covariance matrix adaptation mechanism, is effective when used to solve non-convex and non-linear optimization problems. When applying CMA-ES, there are no bound constraints on the optimization variables.

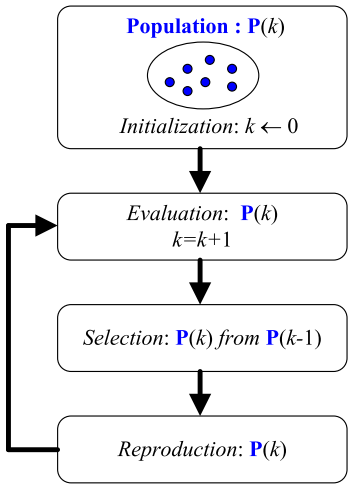

FIGURE 4. Procedure of heuristic optimization methods.

Here, we denote three LQ SOF controllers, $\mathbf{K}_{SOF1}$, $\mathbf{K}_{SOF2}$ and $\mathbf{K}_{SOF3}$, which are obtained by solving (29), as LQSOFq1, LQSOFq2 and LQSOFq3, respectively.

Among the three LQ SOF controllers, $\mathbf{K}_{SOF1}$, $\mathbf{K}_{SOF2}$ and $\mathbf{K}_{SOF3}$, the last is expected to show the best performance in terms of the suspension force, (1). The SOF controller with $\mathbf{K}_{SOF3}$ is represented as (30). By replacing u in (1) with u_{q3}, the suspension force becomes (31). If q_1 and q_2 are set exactly to k_s and b_s respectively, the suspension force will be zero. This means that no forces can be transmitted to the sprung mass through the suspension. As a result, the vertical acceleration will be always zero regardless of the type of road profile. However, this is impossible in actual vehicles because k_s and b_s are not linear and time-varying.

$$\begin{aligned} u_{q3} &= \mathbf{K}_{SOF3}\mathbf{y}_{q3} = \begin{bmatrix} q_1 & q_2 \end{bmatrix}\begin{bmatrix} z_s - z_u \\ \dot{z}_s - \dot{z}_u \end{bmatrix} \\ &= q_1\left(z_s - z_u\right) + q_2\left(\dot{z}_s - \dot{z}_u\right) \quad (30) \\ f &= -k_s(z_s - z_u) - b_s(\dot{z}_s - \dot{z}_u) + u_{q3} \\ &= \left(q_1 - k_s\right)\left(z_s - z_u\right) + \left(q_2 - b_s\right)\left(\dot{z}_s - \dot{z}_u\right) \quad (31) \end{aligned}$$

D. HOW TO CONVERT CONTROLLERS FOR QUARTER-CAR MODEL TO FULL-CAR ONES

As shown in Fig. 2, it can be regarded that the full-car model consists of four quarter-car ones. The vertical displacements of the sprung and unsprung masses, z_{si} and z_{ui}, at each corner in the full-car model are identical to those of the quarter-car model. Thus, the LQR designed with the quarter-car model can be directly applied to derive the LQR for the full-car model. This subsection explains how to convert the LQR for quarter-car model to a full-state feedback controller for the full-car model.

To represent the state vector of (3) with the state variables of (16), the state vector at each corner, $\mathbf{x}_{qi}$, is defined as (32) with certain state variables in the full-car model. By multiplying $\mathbf{K}_q$ and $\mathbf{x}_{qi}$ together as in LQRq, i.e., (7), the control input at each corner is calculated as (33). With $\mathbf{K}_q$ in (7)

and the vectors defined in (14), the vector of control inputs for the full-car model, $\mathbf{u}_f$, is calculated as (34). This has a form identical to that of (33), which is the control input for the quarter-car model. Here, (34) is converted to (35) with (15). The four vectors in (35) can be derived from the state vector of the full-car model, $\mathbf{x}_f$, with the output matrices defined in (36). In (36), $\mathbf{I}$ and $\mathbf{0}$ represent the identity and zero matrices, respectively. With these definitions in (36), the vector of the control inputs for the full-car model is represented as (37) [27]. In (37), the gain matrix $\mathbf{H}$ has a special structure. Hence, it differs from the gain matrix of LQR, $\mathbf{K}_f$. Moreover, there are four distinct elements in $\mathbf{H}$ because those are given from $\mathbf{K}_q$, i.e., the gain matrix of LQR for the quarter-car model. This is relatively few compared to those of $\mathbf{K}_f$. Here, we denote the controller $\mathbf{H}$ as LQRfq.

$$\mathbf{x}_{qi} = \begin{bmatrix} z_{si} & z_{ui} & \dot{z}_{si} & \dot{z}_{ui} \end{bmatrix}^T, \quad i = 1, 2, 3, 4 \tag{32}$$

$$\begin{aligned} u_i &= -\mathbf{K}_q \mathbf{x}_{qi} \\ &= -\left(k_1 z_{si} + k_2 z_{ui} + k_3 \dot{z}_{si} + k_4 \dot{z}_{ui}\right), \quad i = 1, 2, 3, 4 \end{aligned} \tag{33}$$

$$\mathbf{u}_f = -k_1 \mathbf{z}_s - k_2 \mathbf{z}_u - k_3 \dot{\mathbf{z}}_s - k_4 \dot{\mathbf{z}}_u \tag{34}$$

$$\mathbf{u}_f = -k_1 \mathbf{G}^T \mathbf{p} - k_2 \mathbf{z}_u - k_3 \mathbf{G}^T \dot{\mathbf{p}} - k_4 \dot{\mathbf{z}}_u \tag{35}$$

$$\begin{cases} \mathbf{p} = \mathbf{C}_1 \mathbf{x}_f, & \mathbf{C}_1 \triangleq \begin{bmatrix} \mathbf{I}_{3\times 3} & \mathbf{0}_{3\times 11} \end{bmatrix} \\ \dot{\mathbf{p}} = \mathbf{C}_2 \mathbf{x}_f, & \mathbf{C}_2 \triangleq \begin{bmatrix} \mathbf{0}_{3\times 7} & \mathbf{I}_{3\times 3} & \mathbf{0}_{3\times 4} \end{bmatrix} \\ \mathbf{z}_u = \mathbf{C}_3 \mathbf{x}_f, & \mathbf{C}_3 \triangleq \begin{bmatrix} \mathbf{0}_{4\times 3} & \mathbf{I}_{4\times 4} & \mathbf{0}_{4\times 7} \end{bmatrix} \\ \dot{\mathbf{z}}_u = \mathbf{C}_4 \mathbf{x}_f, & \mathbf{C}_4 \triangleq \begin{bmatrix} \mathbf{0}_{4\times 10} & \mathbf{I}_{4\times 4} \end{bmatrix} \end{cases} \tag{36}$$

$$\begin{aligned} \mathbf{u}_f &= -k_1 \mathbf{G}^T \mathbf{C}_1 \mathbf{x}_f - k_2\, \mathbf{C}_3 \mathbf{x}_f - k_3 \mathbf{G}^T \mathbf{C}_2\, \mathbf{x}_f - k_4 \mathbf{C}_4 \mathbf{x}_f \\ &= -\left(k_1 \mathbf{G}^T \mathbf{C}_1 + k_2 \mathbf{C}_3 + k_3 \mathbf{G}^T \mathbf{C}_2 + k_4 \mathbf{C}_4\right) \mathbf{x}_f \\ &= -\mathbf{H} \mathbf{x}_f \end{aligned} \tag{37}$$

Approximating the method of (37), a full-state feedback controller for the full-car model can be derived from the LQ SOF controllers designed with the quarter-car model, i.e., $\mathbf{K}_{SOF1}$, $\mathbf{K}_{SOF2}$ and$\mathbf{K}_{SOF3}$ in (26). For example, the sensor output $\mathbf{y}_{q3}$ given in (25) for the quarter-car model can be represented as (38) for the full-car model. With (38), the LQ SOF controller for the full-car model, $\mathbf{K}_{SOF4}$, is given as (39). The dimension of $\mathbf{K}_{SOF4}$ is 4×8 because that of $\mathbf{y}_{f4}$ is 8. Let define $\mathbf{K}_{SOF3}$ as the vector of two gain elements, q_1 and q_2, as shown in (40). From this definition, $\mathbf{K}_{SOF4}$ is derived as (41) with elements identical to those of $\mathbf{K}_{SOF3}$. Hence, only two elements of $\mathbf{K}_{SOF3}$ are needed when deriving the full-state feedback controller for the full-car model, $\mathbf{K}_{SOF4}$. With the definition of (40), the full-state feedback controller gain $\mathbf{V}_{q3}$ is obtained as (42). In the same manner, $\mathbf{K}_{f4}$ in (39) is derived as (43). Another way to derive $\mathbf{K}_{f4}$ is to use the LQ SOF controller, $\mathbf{V}_{q3}$, obtained in (42). The full-state feedback controller $\mathbf{F}$ is derived as (44) from $\mathbf{V}_{q3}$ of (42) identically to (37). It is natural that $\mathbf{K}_{f4}$ of (39) and $\mathbf{F}$ of (44) are identical to each other. We refer to the controller $\mathbf{K}_{f4}$ as LQSOFfq4.

$$\begin{aligned} \mathbf{y}_{f4} &= \begin{bmatrix} \mathbf{z}_s - \mathbf{z}_u \\ \dot{\mathbf{z}}_s - \dot{\mathbf{z}}_u \end{bmatrix} \\ &= \begin{bmatrix} \mathbf{G}^T & -\mathbf{I}_{4\times 4} & \mathbf{0}_{4\times 3} & \mathbf{0}_{4\times 4} \\ \mathbf{0}_{4\times 3} & \mathbf{0}_{4\times 4} & \mathbf{G}^T & -\mathbf{I}_{4\times 4} \end{bmatrix} \mathbf{x}_f \\ &= \mathbf{C}_{f4} \mathbf{x}_f \end{aligned} \tag{38}$$

$$\mathbf{u}_{f4} = \mathbf{K}_{SOF4} \mathbf{y}_{f4} = \mathbf{K}_{SOF4}\ \mathbf{C}_{f4} \mathbf{x}_f = \mathbf{K}_{f4} \mathbf{x}_f \tag{39}$$

$$\mathbf{K}_{SOF3} = \begin{bmatrix} q_1 & q_2 \end{bmatrix} \tag{40}$$

$$\mathbf{K}_{SOF4} = \begin{bmatrix} q_1 \mathbf{I}_{4\times 4} & q_2 \mathbf{I}_{4\times 4} \end{bmatrix} \tag{41}$$

$$\begin{aligned} \mathbf{V}_{q3} &= \mathbf{K}_{SOF3} \mathbf{C}_{s3} = \begin{bmatrix} q_1 & q_2 \end{bmatrix} \begin{bmatrix} 1 & -1 & 0 & 0 \\ 0 & 0 & 1 & -1 \end{bmatrix} \\ &= \begin{bmatrix} q_1 & -q_1 & q_2 & -q_2 \end{bmatrix} \end{aligned} \tag{42}$$

$$\begin{aligned} \mathbf{K}_{f4} &= \begin{bmatrix} q_1 \mathbf{I}_{4\times 4} & q_2 \mathbf{I}_{4\times 4} \end{bmatrix} \\ &\quad \times \begin{bmatrix} \mathbf{G}^T & -\mathbf{I}_{4\times 4} & \mathbf{0}_{4\times 3} & \mathbf{0}_{4\times 4} \\ \mathbf{0}_{4\times 3} & \mathbf{0}_{4\times 4} & \mathbf{G}^T & -\mathbf{I}_{4\times 4} \end{bmatrix} \\ &= \begin{bmatrix} q_1 \mathbf{G}^T & -q_1 \mathbf{I}_{4\times 4} & q_2 \mathbf{G}^T & -q_2 \mathbf{I}_{4\times 4} \end{bmatrix} \end{aligned} \tag{43}$$

$$\mathbf{u}_{f4} = \left(q_1 \mathbf{G}^T \mathbf{C}_1 - q_1 \mathbf{C}_3 + q_2 \mathbf{G}^T \mathbf{C}_2 - q_2 \mathbf{C}_4\right) \mathbf{x}_f = \mathbf{F} \mathbf{x}_f \tag{44}$$

In (41), the LQ SOF controller for the full-car model, $\mathbf{K}_{SOF4}$, is derived from $\mathbf{K}_{SOF3}$ of the quarter-car model. Another way to design the LQ SOF controller for the full-car model is directly to optimize the controller of (45), which is identical to (41). As shown in (45), there are two decision variables, q_1 and q_2, in the optimization problem. We denote this controller as $\mathbf{K}_{SOF5}$, as shown in (45). The optimization problem with the LQ objective function (20) is formulated as (47). To solve the optimization problem, the heuristic optimization method, CMA-ES, is applied [49]. With the optimized $\mathbf{K}_{SOF5}$, the full-state feedback controller for the full-car model is obtained as (46). We refer to the controller $\mathbf{K}_{f5}$ as LQSOFfq5.

$$\mathbf{K}_{SOF5} = \begin{bmatrix} q_1 \mathbf{I}_{4\times 4} & q_2 \mathbf{I}_{4\times 4} \end{bmatrix} \tag{45}$$

$$\mathbf{u}_{f5} = \mathbf{K}_{SOF5} \mathbf{y}_{f4} = \mathbf{K}_{SOF5}\ \mathbf{C}_{f4} \mathbf{x}_f = \mathbf{K}_{f5} \mathbf{x}_f \tag{46}$$

$$\begin{aligned} &\min_{q_1, q_2} J_{ff} = \frac{1}{2} \text{trace}\left(\mathbf{P}_f\right) \\ &s.t. \begin{cases} \mathbf{P}_f = \mathbf{P}_f^T > \mathbf{0} \\ \max\left(Re\left[\mathbf{A}_f + \mathbf{B}_{2f} \mathbf{K}_{f5}\right]\right) < \mathbf{0} \\ \left(\mathbf{A}_f + \mathbf{B}_{2f} \mathbf{K}_{f5}\right)^T \mathbf{P}_f + \mathbf{P}_f \left(\mathbf{A}_f + \mathbf{B}_{2f} \mathbf{K}_{f5}\right) \\ +\mathbf{Q}_{fq} + \mathbf{K}_{f5}^T \mathbf{N}_{fq}^T + \mathbf{N}_{fq} \mathbf{K}_{f5} + \mathbf{K}_{f5}^T \mathbf{R}_{fq}\ \mathbf{K}_{f5} = \mathbf{0} \end{cases} \end{aligned} \tag{47}$$

The controller LQSOFfq5 is designed with the LQ objective function, (20). In (20), there are no terms on the roll and pitch angles. Therefore, it is expected that LQSOFfq5 has little capability to control the roll and pitch motions of the sprung mass. To control these motions, the controller with the form of $\mathbf{K}_{SOF5}$ in (45) is designed with the LQ objective function, (21). The optimization problem needed to find the controller is identical to (47) except that $\mathbf{Q}_{fq}$, $\mathbf{N}_{fq}$ and $\mathbf{R}_{fq}$ are replaced with $\mathbf{Q}_{fr}$, $\mathbf{N}_{fr}$ and $\mathbf{R}_{fr}$ as given in (21), respectively.

Let the controller obtained by solving this optimization be denoted as LQSOFfr5.

E. LQ SOF CONTROLLER DESIGN WITH FULL-CAR MODEL

If there are identical state variables in the quarter- and full-car models, the controllers obtained from the quarter-car model can be used for the full-car case, as described in the previous subsection. However, this is not possible if the state variables are not common between these models. For instance, the vertical displacement, the roll angle and the pitch angle of the sprung mass cannot be obtained from the quarter-car model. Therefore, it is necessary to design a SOF controller with these sensor outputs defined in the full-car model.

As mentioned in subsection II.C, it is assumed that the roll and pitch rates, the suspension stroke and the corresponding rate can be measured with sensors. Thus, the output matrix is defined as (49). In (49), the row vectors, Φ and Θ, are defined in (48). With the outputs, the LQ SOF controller, $\mathbf{K}_{SOF6}$, for the full-car model is defined as (50). The dimension of $\mathbf{K}_{SOF6}$ is 4×10 because the number of outputs is 10. Accordingly, the LQ SOF controller, $\mathbf{K}_{SOF6}$, has the form of (51). From the geometry of the sprung mass, the roll motion is symmetric with respect to the X axis and the pitch motion is proportional to the ratio of the lengths from the center of gravity to the front and rear axles. For this reason, a single gain is needed for the roll motion, and two gains are needed for the pitch motion. Given these facts, $\mathbf{K}_{SOF6}$ in (51) is converted to (52). As shown in (52), there are five elements of $\mathbf{K}_{SOF6}$ is 5. To find the optimum $\mathbf{K}_{SOF6}$, the optimization problem is formulated as (53). To solve the optimization problem, the heuristic optimization method, CMA-ES, is applied [49]. We refer to the controller $\mathbf{K}_{f6}$ as LQSOFfq6. In (53), $\mathbf{Q}_{fq}$, $\mathbf{N}_{fq}$ and $\mathbf{R}_{fq}$ represent the weighting matrices derived from the LQ objective function (20).

$$\Phi \triangleq \begin{bmatrix} 0 & 1 & 0 \end{bmatrix}, \quad \Theta \triangleq \begin{bmatrix} 0 & 0 & 1 \end{bmatrix} \tag{48}$$

$$\begin{aligned} \mathbf{y}_{f6} &= \begin{bmatrix} \dot{\phi} \\ \dot{\theta} \\ \mathbf{z}_s - \mathbf{z}_u \\ \dot{\mathbf{z}}_s - \dot{\mathbf{z}}_u \end{bmatrix} \\ &= \begin{bmatrix} \mathbf{0}_{1\times3} & \mathbf{0}_{1\times4} & \Phi & \mathbf{0}_{1\times4} \\ \mathbf{0}_{1\times3} & \mathbf{0}_{1\times4} & \Theta & \mathbf{0}_{1\times4} \\ \mathbf{G}^T & -\mathbf{I}_{4\times4} & \mathbf{0}_{4\times3} & \mathbf{0}_{4\times4} \\ \mathbf{0}_{4\times3} & \mathbf{0}_{4\times4} & \mathbf{G}^T & -\mathbf{I}_{4\times4} \end{bmatrix} \mathbf{x}_f \\ &= \mathbf{C}_{f6}\mathbf{x}_f \end{aligned} \tag{49}$$

$$\mathbf{u}_{f6} = \mathbf{K}_{SOF6}\mathbf{y}_{f6} = \mathbf{K}_{SOF6}\ \mathbf{C}_{f6}\mathbf{x}_f = \mathbf{K}_{f6}\mathbf{x}_f \tag{50}$$

$$\mathbf{K}_{SOF6} = \begin{bmatrix} h_1 & h_5 & & \\ h_2 & h_6 & h_9\mathbf{I}_{4\times4} & h_{10}\mathbf{I}_{4\times4} \\ h_3 & h_7 & & \\ h_4 & h_8 & & \end{bmatrix} \tag{51}$$

$$\mathbf{K}_{SOF6} = \begin{bmatrix} -h_1 & h_2 & & \\ h_1 & h_2 & h_4\mathbf{I}_{4\times4} & h_5\mathbf{I}_{4\times4} \\ -h_1 & h_3 & & \\ h_1 & h_3 & & \end{bmatrix} \tag{52}$$

$$\begin{aligned} &\min_{\mathbf{K}_{SOF6}} J_{ff} = \frac{1}{2}\text{trace}\left(\mathbf{P}_f\right) \\ &s.t. \begin{cases} \mathbf{P}_f = \mathbf{P}_f^T > \mathbf{0} \\ \max\left(Re\left[\mathbf{A}_f + \mathbf{B}_{2f}\mathbf{K}_{f6}\right]\right) < 0 \\ \left(\mathbf{A}_f + \mathbf{B}_{2f}\mathbf{K}_{f6}\right)^T \mathbf{P}_f + \mathbf{P}_f \left(\mathbf{A}_f + \mathbf{B}_{2f}\mathbf{K}_{f6}\right) \\ +\mathbf{Q}_{fq}+\mathbf{K}_{f6}^T\mathbf{N}_{fq}^T + \mathbf{N}_{fq}\mathbf{K}_{f6} + \mathbf{K}_{f6}^T\mathbf{R}_{fq}\ \mathbf{K}_{f6} = \mathbf{0} \end{cases} \end{aligned} \tag{53}$$

Although LQSOFfq6 uses the roll and pitch rates for feedback, the LQ objective function (20) used when designing it has no terms on the roll and pitch angles. Hence, it is expected that the control performance for the roll and pitch motions can be improved if the roll and pitch angles are added to the LQ objective function as in (21). For this purpose, the controller with the form of $\mathbf{K}_{SOF6}$ in (52) is designed with the LQ objective function, (21). The optimization problem needed to find the controller is identical to (53) except that $\mathbf{Q}_{fq}$, $\mathbf{N}_{fq}$ and $\mathbf{R}_{fq}$ are replaced with $\mathbf{Q}_{fr}$, $\mathbf{N}_{fr}$ and $\mathbf{R}_{fr}$ in (21), respectively. Let the controller obtained by solving this optimization be denoted as LQSOFfr6.

III. FREQUENCY DOMAIN ANALYSIS AND SIMULATION

In this section, a frequency-domain analysis and a simulation are conducted to assess the performance of the designed LQ SOF controllers. Through the frequency-domain analysis and simulation, the designed SOF controllers are compared to one another.

Table 1 shows the parameter descriptions and the corresponding values of the 2-DOF quarter-car and 7-DOF full-car models, as referenced from Demo_Lexus_NX300h given in CarMaker. The weights in the LQ objective functions, (5), (18), (20) and (21), are calculated using (6) with the maximum allowable values given in Table 2. The set of weights given in Table 2 emphasizes ride comfort, i.e., a reduction of the vertical acceleration of the sprung mass. In consequence, road adhesion is degraded. In this paper, it is assumed that the actuator has an infinite bandwidth during the generation of the active control force. Table 3 shows the controller gain matrices of the designed controllers.

A. FREQUENCY RESPONSE ANALYSIS WITH QUARTER-CAR AND FULL-CAR MODELS

The first type of frequency-domain analysis is done with the quarter-car model for LQRq, LQSOFq1, LQSOFq2 and LQSOFq3. Fig. 5 shows the frequency responses of each output from the road profile z_r with the quarter-car model for each controller.

As shown in Fig. 5-(a), LQSOFq3 shows the best performance in terms of ride comfort among the LQ SOF controllers, as given in (26). Looking at this another way, LQSOFq3 shows performance nearly similar to that of LQRq within the frequency range of 4 to 10Hz. Moreover, LQSOFq3 shows the best performance in terms of road adhesion, as shown in Fig. 5-(d). This is expected from (31). On the other hand, the height of the sprung mass with LQSOFq3 is worse than that with the passive suspension system below 0.6Hz, as shown in Fig. 5-(b).

TABLE 1. Parameter descriptions and the corresponding values of the 2-DOF quarter-car and 7-DOF full-car models.

m_s	Sprung mass of the full-car model	1,950.0 kg
m_q	Sprung mass of the quarter-car model	$m_s/4$
m_{u1}, m_{u2}, m_{u3}, m_{u4}	Unsprung masses of the full-car model	62.0 kg
I_x	Roll moment of inertia of the sprung mass in the full-car model	703.7 kg·m^2
I_y	Pitch moment of inertial of the sprung mass in the full-car model	2,358.0 kg·m^2
k_{s1}, k_{s2}	Spring stiffness of the front suspensions in the full-car model	35,000 N/m
k_{s3}, k_{s4}	Spring stiffness of the rear suspensions in the full-car model	45,000 N/m
b_{s1}, b_{s2}, b_{s3}, b_{s4}	Damping coefficients of the suspensions in the full-car model	3,500 N·s/m
k_{t1}, k_{t2}, k_{t3}, k_{t4}	Tire stiffness of the suspensions in the full-car model	391,961 N/m
k_s	Spring stiffness of the quarter-car model	35,000 N/m
b_s	Damping coefficients of the quarter-car model	3,500 N·s/m
k_t	Tire stiffness of the quarter-car model	391,961 N/m
l_f	Distance from C.G. to the front suspensions	1.172 m
l_r	Distance from C.G. to the rear suspensions	1.488 m
t_f, t_r	Half of treads of the front and rear axles in the full-car model	0.785 m

TABLE 2. Maximum allowable values in LQ objective function.

η_1	1.0 m/s^2	η_2	0.2 m	η_3	0.2 m
η_4	3,000 N	η_5	10 deg/s^2	η_6	10 deg/s^2
η_7	3 deg	η_8	10 deg/s	η_9	3 deg
η_{10}	10 deg/s				

TABLE 3. Controller gain matrices of each controller.

$\mathbf{K}_q$	$[-28929.0 \quad 31605.0 \quad -1533.4 \quad 3019.5]$
$\mathbf{K}_{SOF1}$	$[-380.9 \quad -234.0]$
$\mathbf{K}_{SOF2}$	$[-353.2 \quad 2273.2]$
$\mathbf{K}_{SOF3}$	$[31336.0 \quad 2991.7]$
$\mathbf{K}_{SOF5}$	$[32007.0\mathbf{I}_{4\times4} \quad 3037.0\mathbf{I}_{4\times4}]$
$\mathbf{K}_{SOF6}$	$\begin{bmatrix} -633.2 & 1121.5 \\ 633.2 & 1121.5 \\ -633.2 & -1229.3 \\ 633.2 & -1229.3 \end{bmatrix} \quad 31112.0\mathbf{I}_{4\times4} \quad 3075.9\mathbf{I}_{4\times4}$

Accordingly, LQSOFq3 can worsen the ride comfort compared to that by the passive suspension system with a low-frequency road profile. LQSOFq1 and LQSOFq2 use the vertical acceleration for the SOF controller. Both outperform the passive suspension system. However, it is not satisfactory over LQRq or LQSOFq3. Thus, it is recommended that the vertical acceleration not be used for the LQ SOF controller when trying to enhance the ride comfort. From these results, it can be concluded that the LQ SOF controller designed with the suspension stroke and the corresponding rate shows the best performance in terms of ride comfort.

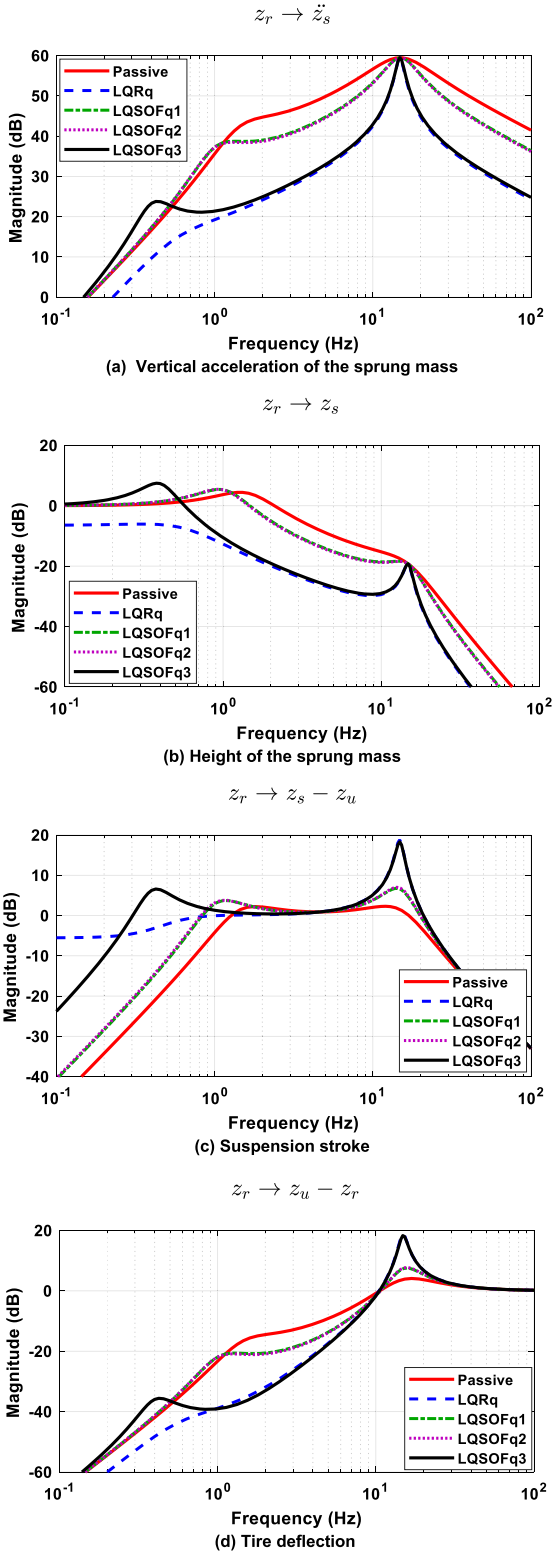

FIGURE 5. Frequency responses from the road profile z_r to each output with the quarter-car model for LQR and LQ SOF controllers.

The second type of frequency-domain analysis is done with the full-car model for LQRfq, LQSOFfq4, LQSOFfq5 and LQSOFfq6. Fig. 6 shows the frequency responses of each

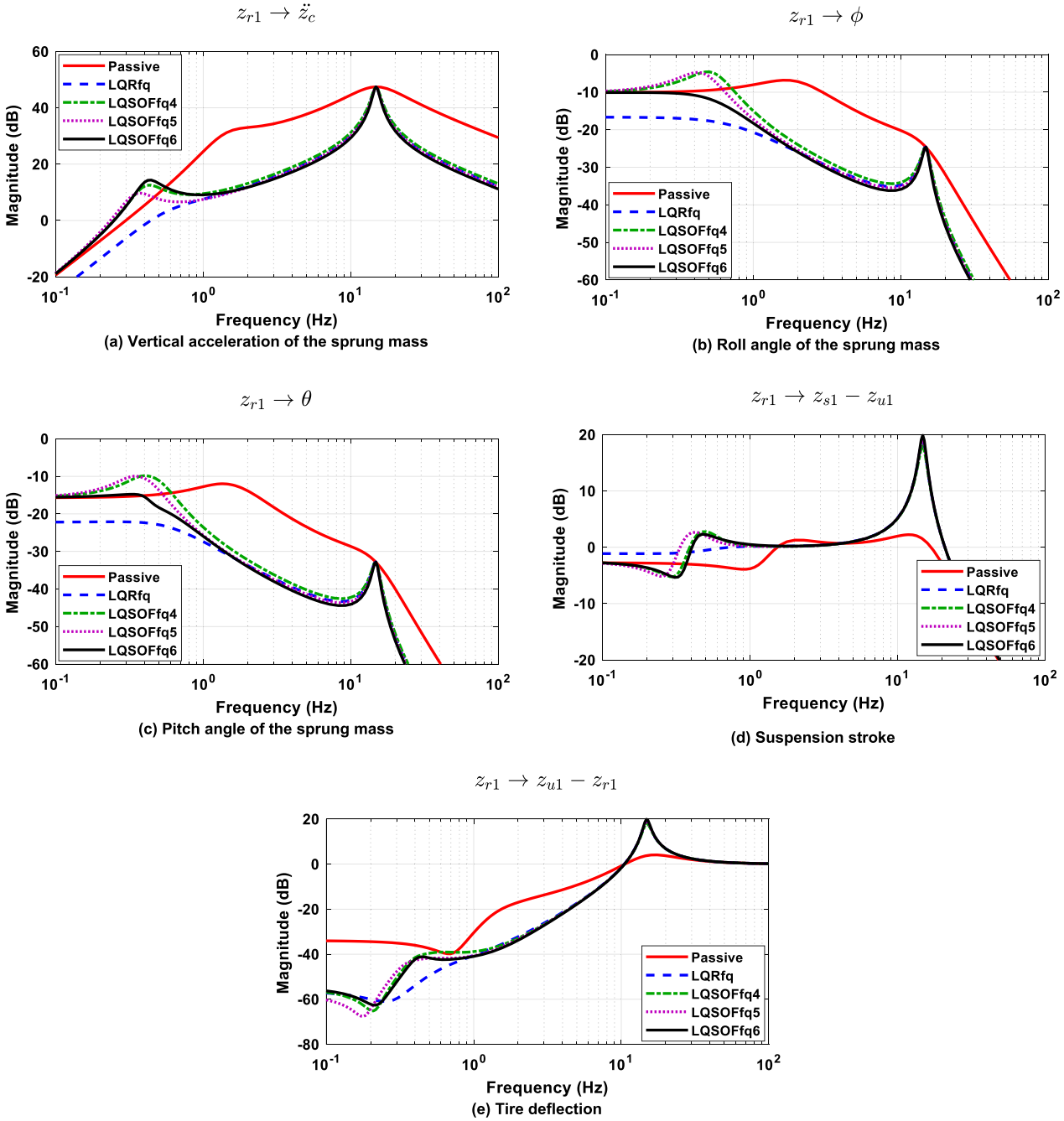

FIGURE 6. Frequency responses from the road profile z_{r1} to each output for controllers with the full-car model.

output from the road profile z_{r1} with the full-car model for each controller. In previous research, it was demonstrated that LQRfq, derived from LQRq, can give performance equivalent to that by LQRf2 with regard to improving the ride comfort [12]. Therefore, LQRq can be used as a reference when comparing the LQ SOF controllers.

As shown in Fig. 6, the LQ SOF controllers show performance similar to that of LQRfq in terms of ride comfort within the frequency range of 4 to 10Hz, which is equivalent to the relationship between LQRq and LQSOFq3 as given in Fig. 5. This stems from the fact that LQRfq and LQSOFfq3 for the full-car model are based on LQRq and LQSOFq3 of the quarter-car model, respectively. As shown in Figs. 6-(b) and -(c), the roll and pitch angles of LQSOFfq4 and LQSOFfq5 become worse than those of LQSOFfq6 for the frequency range below 1Hz. This indicates that the ride comfort along the horizon direction is degraded by those controllers. Compared to LQSOFfq4 and LQSOFfq5,

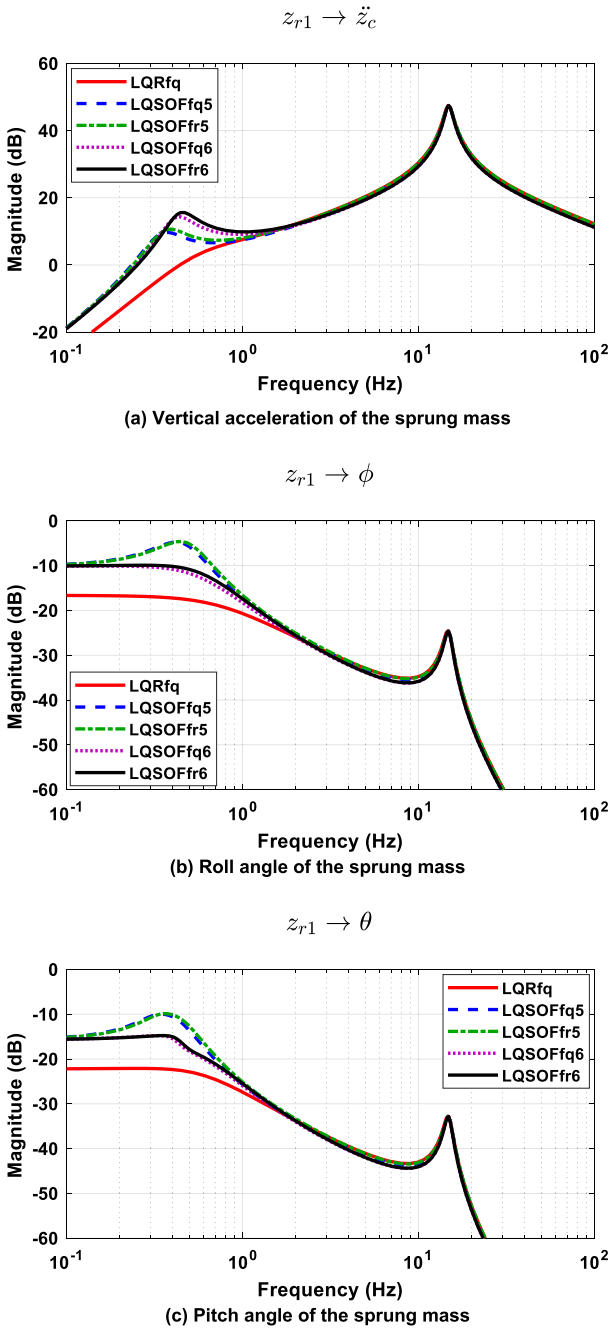

FIGURE 7. Frequency responses from the road profile z_{r1} to each output for controllers with the full-car model.

LQSOFfq6 shows better performance with regard to controlling the roll and pitch motions because the roll and pitch rates are used for feedback. On the other hand, the suspension strokes and the tire deflections of the LQ SOF controllers are nearly identical to one another, as shown in Figs. 6-(d) and -(e). It should also be noted that LQRfq shows the best performance when used to control the roll and pitch motions of the sprung mass, as shown in Figs. 6-(b) and (c), despite the fact that there are no terms on the roll and pitch angles in the LQ objective function of LQRq, (5).

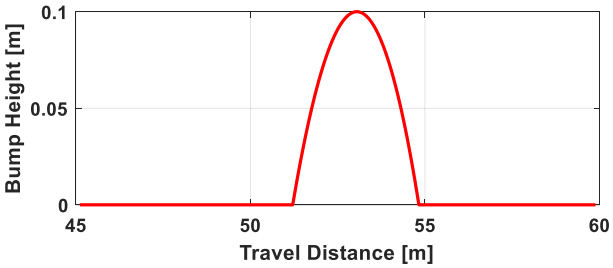

FIGURE 8. Single bump profile.

From these results, it is demonstrated that LQSOFfq6 with the roll and pitch rates shows the best performance among the LQ SOF controllers in terms of ride comfort along the horizontal direction. Moreover, it is better to use the roll and pitch rates for the LQ SOF controllers.

To check the effects of the roll and pitch angles in the LQ objective function and the roll and pitch rates in the feedback controller on the control performance, frequency responses are drawn with the full-car model for LQSOFfq5, LQSOFfr5, LQSOFfq6 and LQSOFfr6. LQRfq is used as a reference. Fig. 7 shows the frequency responses from the road profile z_{r1} to each output for those controllers. In contrast to Fig. 6, the suspension stroke and tire deflection are not presented given the similarity to those in Fig. 6.

As shown in Fig. 7, there are few differences between LQSOFfq5 and LQSOFfr5, and between LQSOFfq6 and LQSOFfr6. These results mean that there are scant effects when adding new terms such as the roll and pitch angles to the LQ objective function and that it is effective to use the roll and pitch rates as signals for feedback. In other words, there are few differences between the LQ objective functions, (20) and (21), if the controller structure is identical or the signals used for feedback are identical. Moreover, if additional signals such as the roll and pitch rates given in (49) are used for feedback control, it has a positive effect on the control performance, as shown in Figs. 7-(b) and -(c). However, it has a side effect in that the vertical accelerations of LQSOFfq6 and LQSOFfr6 deteriorate in the low frequency range below 1Hz, as given in Fig. 7-(a). This stems from the fact that two new terms are added to the LQ objective function, (20).

B. SIMULATION ON CARMAKER

The simulation is conducted on the vehicle simulation package IPG CarMaker for the designed controllers under disturbances of single and sine-sweep bump profiles. Two sets of controllers are used for the simulation. The first set includes the passive system, LQRq, LQSOFq1, LQSOFq2 and LQSOFq3. The second set includes LQRq, LQSOFq3 and LQSOFfq6.

The vehicle model is Demo_Lexus_NX300h, given by default in CarMaker. In this model, the spring stiffness and damping coefficient are nonlinear. Fig. 8 shows the single bump profile used for the simulation. The vehicle starts at

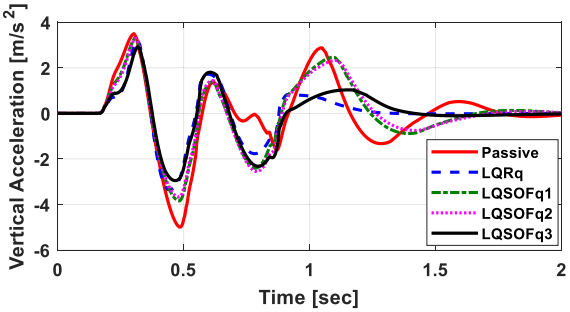

(a) Vehicle acceleration of the sprung mass

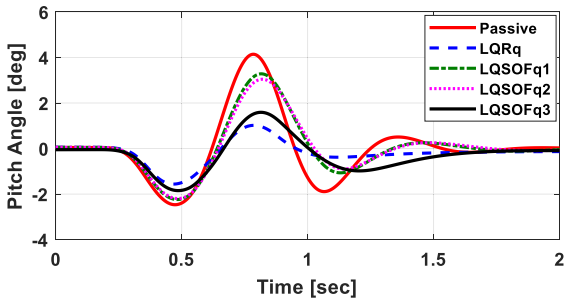

(b) Pitch angle of the sprung mass

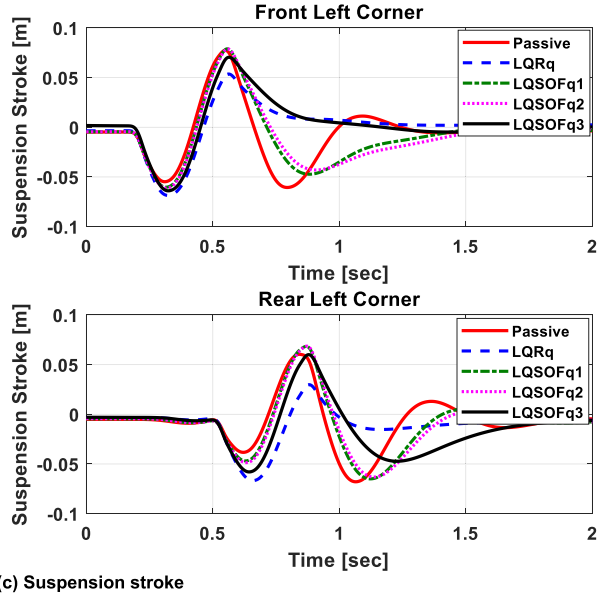

(c) Suspension stroke

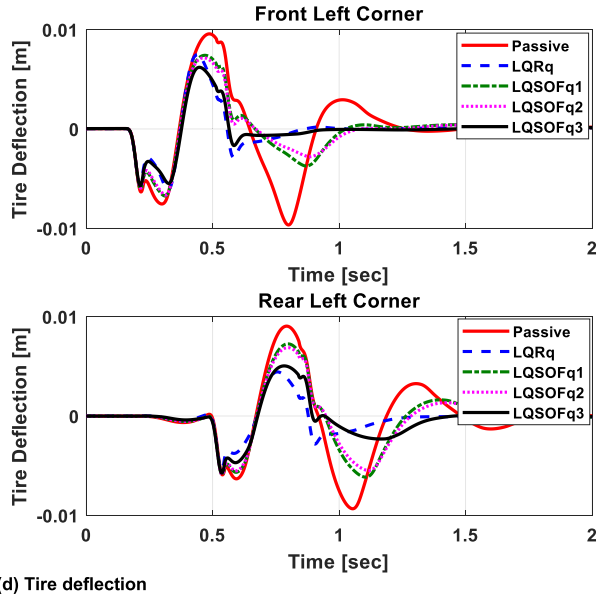

(d) Tire deflection

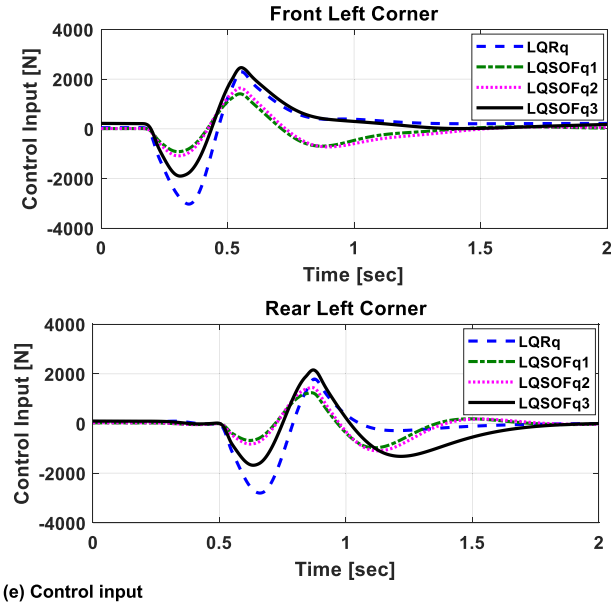

(e) Control input

FIGURE 9. Simulation results obtained from CarMaker for each controller.

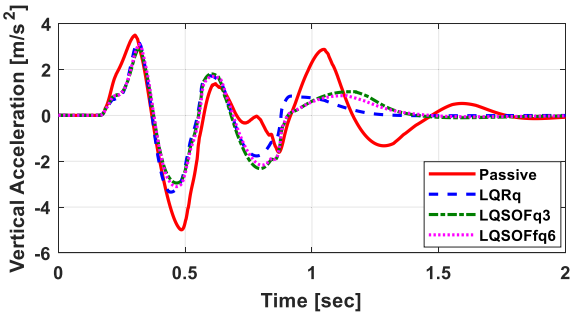

(a) Vehicle acceleration of the sprung mass

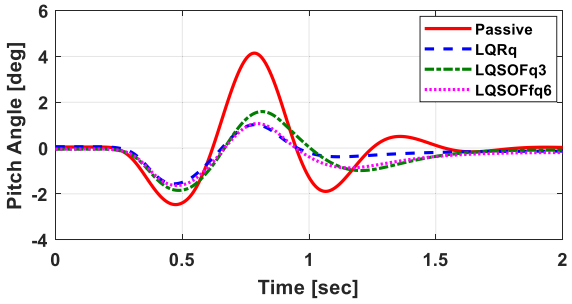

(b) Pitch angle

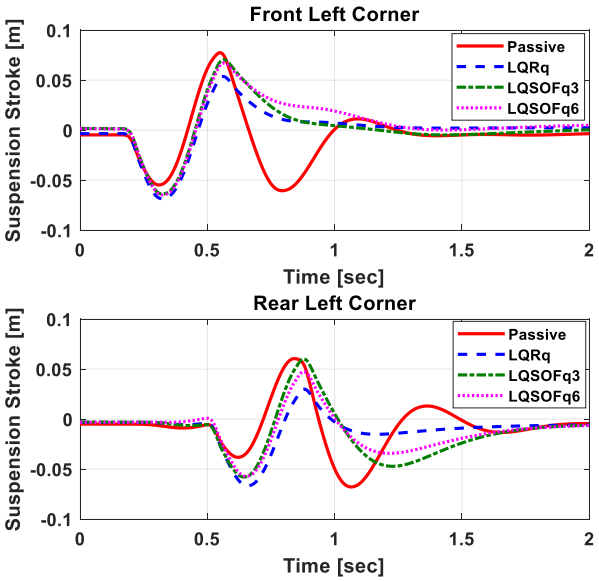

(c) Suspension stroke

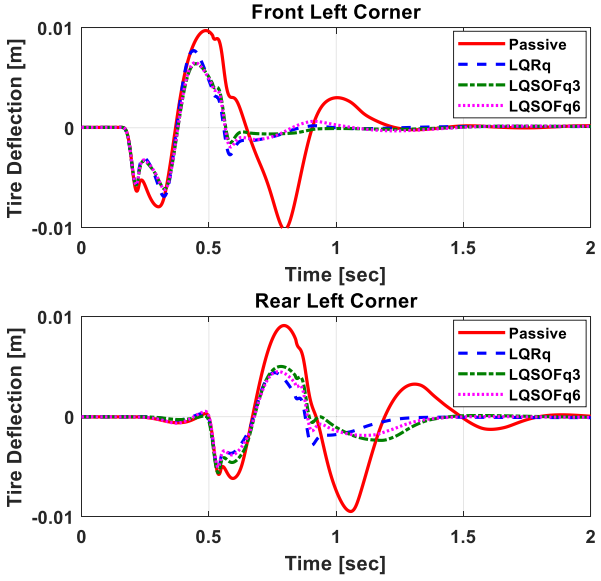

(d) Tire deflection

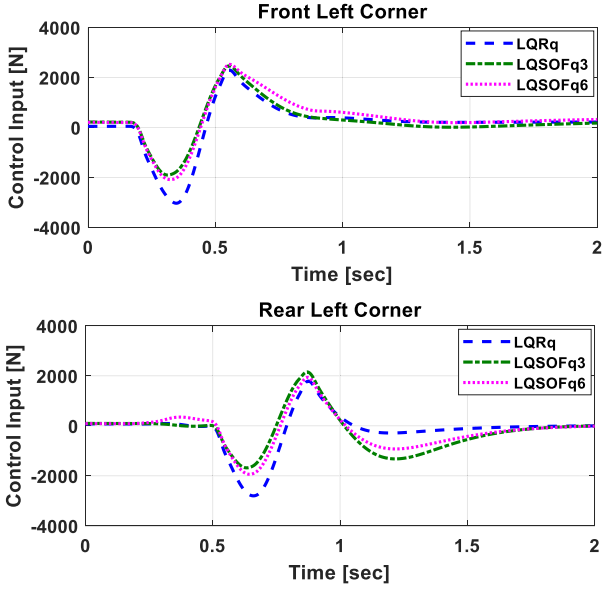

(e) Control input

FIGURE 10. Simulation results obtained from CarMaker for each controller.

TABLE 4. Peak-to-peak values of responses for each controller at front right corner.

	$\ddot{z}_c$ (m/s^2)	θ (deg)	SS (m)	TD (m)	Control input (N)
Passive	8.5	6.6	0.138	0.019	0
LQRq	6.6	4.0	0.154	0.014	5678
LQSOFq1	7.2	5.5	0.139	0.014	2330
LQSOFq2	7.0	5.2	0.140	0.014	2728
LQSOFq3	5.9	4.8	0.153	0.012	4926
LQSOFfq6	6.2	4.2	0.153	0.013	5035

TABLE 5. Root-mean-square values of responses for each controller at front right corner.

	$\ddot{z}_c$ (m/s^2)	θ (deg)	SS (m)	TD (m)	Control input (N)
Passive	1.53	1.45	0.028	0.004	0
LQRq	1.08	0.56	0.023	0.002	993
LQSOFq1	1.41	1.21	0.029	0.003	473
LQSOFq2	1.40	1.15	0.030	0.003	555
LQSOFq3	1.11	0.81	0.025	0.002	839
LQSOFfq6	1.10	0.67	0.026	0.002	962

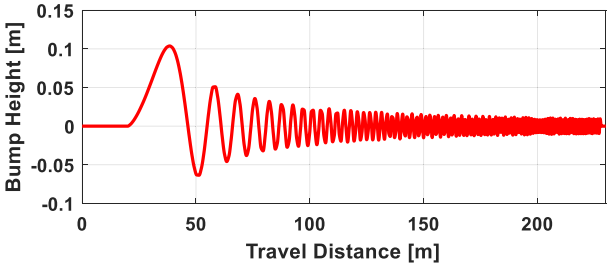

FIGURE 11. Sine-sweep bump.

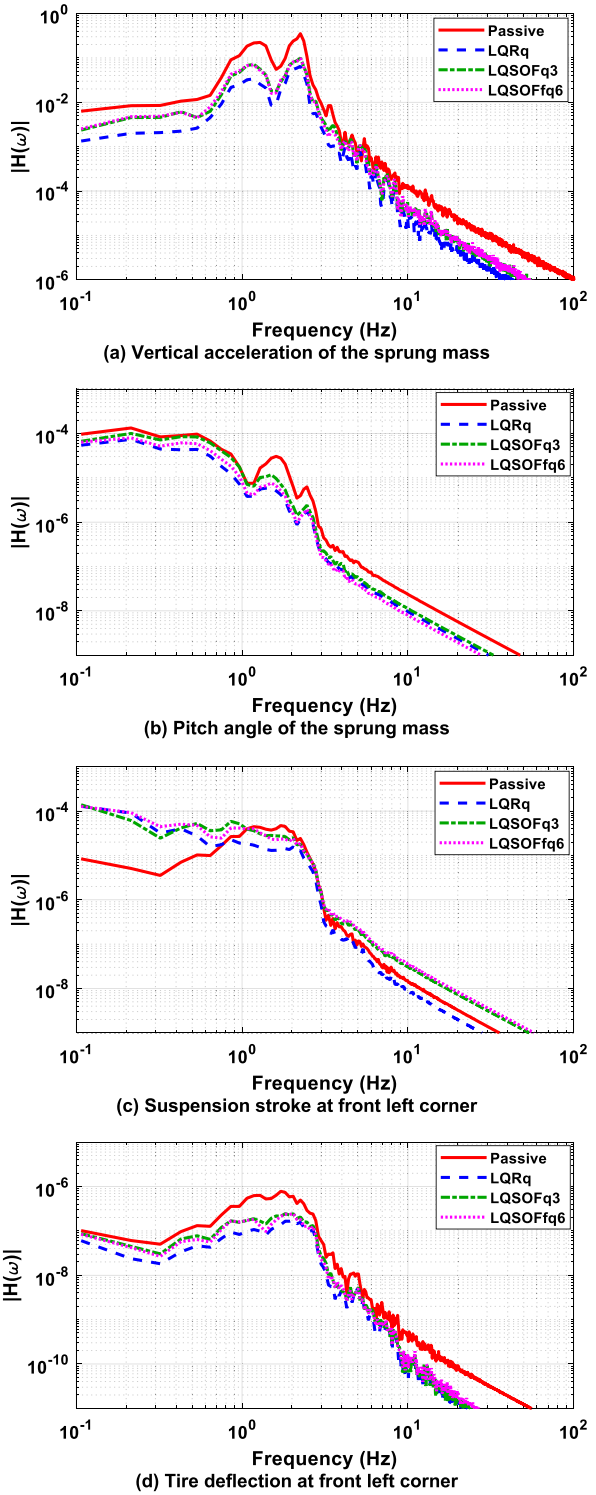

FIGURE 12. Frequency responses obtained from CarMaker for each controller on the sine-sweep bump.

stand-still position and accelerates at 30km/h according to the built-in speed controller in CarMaker. The vehicle then passes a bump. The tire-road friction coefficient is set to 0.8. There are slight roll motions because the bump is evenly applied to the left and right wheels. As mentioned earlier, it is assumed that the actuator used for active suspension has an infinite bandwidth in the generation of the control input.

Fig. 9 shows the simulation results for the first set of LQ SOF controllers. As shown in Fig. 9, LQRq shows the best performance in terms of ride comfort. This is expected from the frequency response of Fig. 5. As expected from the frequency response of Fig. 5-(a), LQSOFq3 shows the best performance in terms of ride comfort among the LQ SOF controllers. As a result of the improved ride comfort, the suspension stroke increases and the tire deflection becomes smaller, as given in Figs. 8-(c) and -(d). As shown in Fig. 9-(e), the control inputs of LQSOFq3 are larger than those of the other LQ SOF controllers. This causes the large suspension stroke and the small amount of vertical acceleration. As shown in Fig. 9-(b), there are slight differences among the pitch angles of the three LQ SOF controllers. This is expected from Fig. 6-(c), which means that LQSOFq3 is not capable

of controlling the roll and pitch motions of the sprung mass. As expected form Fig. 6-(c), LQRq shows the best performance for control of the pitch motion of the sprung mass despite the fact that there is no term on the pitch angle in the LQ objective function of LQRq, (5).

Fig. 10 shows the simulation results for the second set of LQ SOF controllers. The difference between LQSOFq3 and LQSOFfq6 is that the latter uses the roll and pitch rates for feedback. The simulation results of LQRq and LQSOFq3 are identical to those given in Fig. 9.

As shown in Fig. 10-(a), the three controllers show good performance in terms of ride comfort. As expected from the frequency response presented in Fig. 6-(a), two LQ SOF controllers shows nearly identical performance in terms of ride comfort. As a result of the improved ride comfort, the suspension stroke and tire deflection increase, as given in Figs. 10-(c) and -(d). As shown in Fig. 10-(b), the pitch angle of LQSOFfq6 is smaller than that of LQSOFq3. This is expected from Fig. 6-(c). In other words, feedback control with the roll and pitch rates can improve the control performance in the roll and pitch motions. As a result, the control inputs of LQSOFfq6 are larger than those of LQSOFq3, as shown in Fig. 10-(e). From these results, it is recommended that the roll and pitch rates be used for feedback control in order to control the roll and pitch motions.

Tables 4 and 5 correspondingly show the peak-to-peak and root-mean-square values of the responses of Figs. 9 and 10 for each controller at front left corner. In Tables 4 and 5, SS and TD denote the suspension stroke and the tire deflection at front left corner, respectively. As shown in Tables 4 and 5, LQRq, LQSOFq3 and LQSOFfq6 show smaller vertical acceleration values than LQSOFq1 and LQSOFq2. In terms of the pitch angle, LQRq shows the best performance although it generates the largest control input. Compared to LQSOFq3, LQSOFfq6 gives the smaller pitch angle because it uses the roll and pitch rates for feedback. However, the control input of LQSOFfq6 increases as a result than LQSOFq3 instead of reducing the pitch angle. In summary, LQSOFfq6 shows good performance in terms of ride comfort, i.e., vertical acceleration and the pitch angle, comparable to LQRq. Moreover, LQSOFq3 is also a good choice given that there are only two elements.

Fig. 11 shows the sine-sweep bump used in the CarMaker simulation. This bump profile can generate a wide range of frequencies. The simulation was done with the controllers LQRq, LQSOFq3 and LQSOFfq6. Fig. 12 shows the frequency responses obtained from the CarMaker simulation for each controller on the sine-sweep bump. As shown in Fig. 12, LQRq shows the best performance in terms of ride comfort. LQSOFq3 and LQSOFfq6 show nearly identical performance in terms of ride comfort. As shown in Fig. 12-(b), LQSOFfq6 shows better performance when used to control the pitch motion of the sprung mass as compared to that by LQSOFq3. These results are identical to those given in Fig. 10 and Tables 4 and 5.

IV. CONCLUSION

In this paper, LQ SOF controllers were designed with a quarter-car model for an active suspension system in order to cope with the problem of measuring the state variables and of implementing the controllers on actual vehicles. These controllers have only two gain elements, and these were used for the quarter-car and full-car models. Therefore, it is easy to implement these controllers on actual vehicles or in vehicle simulation packages. From the definition of the suspension force, the LQ SOF controller with the suspension stroke and the corresponding rate was expected to show the best performance in terms of ride comfort. To find the gains of the LQ SOF controllers, an optimization problem was formulated and solved by the heuristic optimization method. The designed LQ SOF controllers were applied to a full-car model. Another LQ SOF controller with five gain elements was also designed with available sensor signals, i.e., roll and pitch rates, in the full-car model in order to improve the control performance during roll and pitch motions. To verify the performance of the designed LQ SOF controllers, a frequency-domain analysis and a simulation with a vehicle simulation package, CarMaker, were conducted. From the analysis and simulation results, it can be concluded that the LQ SOF controller with two gain elements showed the best performance in terms of ride comfort. Moreover, it is desirable to add new signals to a feedback controller to improve the control performance under roll and pitch motions instead of adding new terms to the LQ objective function. The drawbacks of the method proposed in this paper are measurements on suspension stroke and limitations on actuator performance. There are several problems in measuring the suspension stroke due to sensor noise, sampling bandwidth and cost, etc. An actuator used in actual vehicles has several limitations on maximum force, bandwidth and maximum moving velocity. Further research can include these topics. Moreover, it can cover parameter estimation of the suspension stiffness and damping coefficient needed to ensure that the suspension force is zero.

REFERENCES

[1] H. E. Tseng and D. Hrovat, "State of the art survey: Active and semi-active suspension control," *Vehicle Syst. Dyn.*, vol. 53, no. 7, pp. 1034–1062, 2015, doi: 10.1080/00423114.2015.1037313.
[2] *Mechanical Vibration and Shock—Evaluation of Human Exposure to Whole-Body Vibration—Part 1: General Requirements, International Organization for Standardization*, Standard ISO 2631-1, Geneva, Switzerland, 1997.
[3] A. N. Rimell and N. J. Mansfield, "Design of digital filters for frequency weightings required for risk assessments of workers exposed to vibration," *Ind. Health*, vol. 45, no. 4, pp. 512–519, 2007, doi: 10.2486/indhealth.45.512.
[4] T. Tseng and D. Hrovat, "Some characteristics of optimal vehicle suspensions based on quarter-car models," in *Proc. 29th IEEE Conf. Decis. Control*, Dec. 1990, pp. 2232–2237, doi: 10.1109/CDC.1990.204022.
[5] M. Ö. Yatak and F. Şahin, "Ride comfort-road holding trade-off improvement of full vehicle active suspension system by interval type-2 fuzzy control," *Eng. Sci. Technol., Int. J.*, vol. 24, no. 1, pp. 259–270, Feb. 2021, doi: 10.1016/j.jestch.2020.10.006.
[6] W. Sun, H. Pan, Y. Zhang, and H. Gao, "Multi-objective control for uncertain nonlinear active suspension systems," *Mechatronics*, vol. 24, no. 4, pp. 318–327, 2014, doi: 10.1016/j.mechatronics.2013.09.009.

[7] L.-X. Guo and L.-P. Zhang, "Robust H_∞ control of active vehicle suspension under non-stationary running," *J. Sound Vibrat.*, vol. 331, no. 26, pp. 5824–5837, Dec. 2012, doi: 10.1016/j.jsv.2012.07.042.

[8] R. Wang, H. Jing, F. Yan, H. Reza Karimi, and N. Chen, "Optimization and finite-frequency H_∞ control of active suspensions in in-wheel motor driven electric ground vehicles," *J. Franklin Inst.*, vol. 352, no. 2, pp. 468–484, Feb. 2015, doi: 10.1016/j.jfranklin.2014.05.005.

[9] H. Pan, W. Sun, X. Jing, H. Gao, and J. Yao, "Adaptive tracking control for active suspension systems with non-ideal actuators," *J. Sound Vibrat.*, vol. 399, pp. 2–20, Jul. 2017, doi: 10.1016/j.jsv.2017.03.011.

[10] Y. Qin, J. J. Rath, C. Hu, C. Sentouh, and R. Wang, "Adaptive nonlinear active suspension control based on a robust road classifier with a modified super-twisting algorithm," *Nonlinear Dyn.*, vol. 97, no. 4, pp. 2425–2442, Sep. 2019, doi: 10.1007/s11071-019-05138-8.

[11] F. Beltran-Carbajal, A. Valderrabano-Gonzalez, A. Favela-Contreras, J. L. Hernandez-Avila, I. Lopez-Garcia, and R. Tapia-Olvera, "An active vehicle suspension control approach with electromagnetic and hydraulic actuators," *Actuators*, vol. 8, no. 2, p. 35, Apr. 2019, doi: 10.3390/act8020035.

[12] J. Wang, F. Jin, L. Zhou, and P. Li, "Implementation of model-free motion control for active suspension systems," *Mech. Syst. Signal Process.*, vol. 119, pp. 589–602, Mar. 2019, doi: 10.1016/j.ymssp.2018.10.004.

[13] X. Shao, F. Naghdy, H. Du, and H. Li, "Output feedback H_∞ control for active suspension of in-wheel motor driven electric vehicle with control faults and input delay," *ISA Trans.*, vol. 92, pp. 94–108, Sep. 2019, doi: 10.1016/j.isatra.2019.02.016.

[14] X. Shao, F. Naghdy, H. Du, and Y. Qin, "Coupling effect between road excitation and an in-wheel switched reluctance motor on vehicle ride comfort and active suspension control," *J. Sound Vibrat.*, vol. 443, pp. 683–702, Mar. 2019, doi: 10.1016/j.jsv.2018.12.012.

[15] W. Li, Z. Xie, P. K. Wong, Y. Cao, X. Hua, and J. Zhao, "Robust non-fragile H_∞ optimum control for active suspension systems with time-varying actuator delay," *J. Vibrat. Control*, vol. 25, no. 18, pp. 2435–2452, Sep. 2019, doi: 10.1177/1077546319857338.

[16] J. J. Rath, M. Defoort, C. Sentouh, H. R. Karimi, and K. C. Veluvolu, "Output-constrained robust sliding mode based nonlinear active suspension control," *IEEE Trans. Ind. Electron.*, vol. 67, no. 12, pp. 10652–10662, Dec. 2020, doi: 10.1109/TIE.2020.2978693.

[17] J. Na, Y. Huang, X. Wu, Y.-J. Liu, Y. Li, and G. Li, "Active suspension control of quarter-car system with experimental validation," *IEEE Trans. Syst., Man, Cybern. Syst.*, early access, Sep. 6, 2021, doi: 10.1109/TSMC.2021.3103807.

[18] W. Sun, H. Gao, and O. Kaynak, "Adaptive backstepping control for active suspension systems with hard constraints," *IEEE/ASME Trans. Mechatronics*, vol. 18, no. 3, pp. 1072–1079, Jun. 2013, doi: 10.1109/TMECH.2012.2204765.

[19] T. P. J. van der Sande, B. L. J. Gysen, I. J. M. Besselink, J. J. H. Paulides, E. A. Lomonova, and H. Nijmeijer, "Robust control of an electromagnetic active suspension system: Simulations and measurements," *Mechatronics*, vol. 23, no. 2, pp. 204–212, Mar. 2013, doi: 10.1016/j.mechatronics.2012.07.002.

[20] X. Zheng, H. Zhang, H. Yan, F. Yang, Z. Wang, and L. Vlacic, "Active full-vehicle suspension control via cloud-aided adaptive backstepping approach," *IEEE Trans. Cybern.*, vol. 50, no. 7, pp. 3113–3124, Jul. 2020, doi: 10.1109/TCYB.2019.2891960.

[21] Q. Guo, D. Zhao, X. Zhao, Z. Li, and X. Shi, "Active suspension control strategy of multi-axle emergency rescue vehicle based on inertial measurement unit," *Sensors*, vol. 21, no. 20, p. 6877, Oct. 2021, doi: 10.3390/s21206877.

[22] R. S. Sharp and D. A. Crolla, "Road vehicle suspension system design—A review," *Vehicle Syst. Dyn.*, vol. 16, no. 3, pp. 167–192, Jan. 1987, doi: 10.1080/00423118708968877.

[23] D. Hrovat, "Survey of advanced suspension developments and related optimal control applications," *Automatica*, vol. 33, no. 10, pp. 1781–1817, 1997, doi: 10.1016/S0005-1098(97)00101-5.

[24] D. Cao, X. Song, and M. Ahmadian, "Editors' perspectives: Road vehicle suspension design, dynamics, and control," *Vehicle Syst. Dyn.*, vol. 49, nos. 1–2, pp. 3–28, Feb. 2011, doi: 10.1080/00423114.2010.532223.

[25] C. Poussot-Vassal, C. Spelta, O. Sename, S. M. Savaresi, and L. Dugard, "Survey and performance evaluation on some automotive semi-active suspension control methods: A comparative study on a single-corner model," *Annu. Rev. Control*, vol. 36, no. 1, pp. 148–160, Apr. 2012, doi: 10.1016/j.arcontrol.2012.03.011.

[26] J. Theunissen, A. Tota, P. Gruber, M. Dhaens, and A. Sorniotti, "Preview-based techniques for vehicle suspension control: A state-of-the-art review," *Annu. Rev. Control*, vol. 51, pp. 206–235, 2021, doi: 10.1016/j.arcontrol.2021.03.010.

[27] M. Park and S. Yim, "Design of static output feedback and structured controllers for active suspension with quarter-car model," *Energies*, vol. 14, no. 24, p. 8231, Dec. 2021, doi: 10.3390/en14248231.

[28] D. A. Wilson, R. S. Sharp, and S. A. Hassan, "The application of linear optimal control theory to the design of active automotive suspensions," *Vehicle Syst. Dyn.*, vol. 15, no. 2, pp. 105–118, Jan. 1987, doi: 10.1080/00423118608968846.

[29] A. Hać, "Optimal linear preview control of active vehicle suspension," *Vehicle Syst. Dyn.*, vol. 21, no. 1, pp. 167–195, Jan. 1992, doi: 10.1080/00423119208969008.

[30] A. G. Ulsoy, D. Hrovat, and T. Tseng, "Stability robustness of LQ and LQG active suspensions," *J. Dyn. Syst., Meas., Control*, vol. 116, no. 1, pp. 123–131, Mar. 1994, doi: 10.1115/1.2900666.

[31] J. F. Camino, D. E. Zampieri, and P. L. D. Peres, "Design of a vehicular suspension controller by static output feedback," *Proc. Amer. Control Conf.*, San Diego, CA, USA, Jun. 1999, pp. 3168–3171, doi: 10.1109/ACC.1999.782348.

[32] M. M. Elmadany and M. I. Al-Majed, "Quadratic synthesis of active controls for a quarter-car model," *J. Vibrat. Control*, vol. 7, no. 8, pp. 1237–1252, Nov. 2001, doi: 10.1177/107754630100700806.

[33] A. E. Bryson and Y. Ho, *Applied Optimal Control*. New York, NY, USA: Taylor & Francis Group, 1975, p. 149.

[34] M. Sunar and S. S. Rao, "Optimal selection of weighting matrices in integrated design of structures/controls," *AIAA J.*, vol. 31, no. 4, pp. 714–720, Apr. 1993, doi: 10.2514/3.49018.

[35] Y. Ochi and K. Kanai, "A new way of pole placement in LQR and its application to flight control," in *Proc. Guid., Navigat. Control Conf.*, Aug. 1993, pp. 1295–1301, doi: 10.2514/6.1993-3845.

[36] T. Hiroe, T. Morimoto, S. Inoue, and H. Takamatsu, "A new method for selecting weighting matrices of LQ regulators and its application to an industrial turbine," in *Proc. 32nd IEEE Conf. Decis. Control*, Dec. 1993, pp. 3333–3334, doi: 10.1109/CDC.1993.325827.

[37] J. W. Choi and Y. B. Seo, "LQR Design with eigenstructure assignment capability," *IEEE Trans. Aerosp. Electron. Syst.*, vol. 35, no. 2, pp. 700–708, Apr. 1999, doi: 10.1109/7.766949.

[38] V. L. Syrmos, C. T. Abdallah, P. Dorato, and K. Grigoriadis, "Static output feedback–s-A survey," *Automatica*, vol. 33, no. 2, pp. 125–137, 1997, doi: 10.1016/S0005-1098(96)00141-0.

[39] M. S. Sadabadi and D. Peaucelle, "From static output feedback to structured robust static output feedback: A survey," *Annu. Rev. Control*, vol. 42, pp. 11–26, Jan. 2016, doi: 10.1016/j.arcontrol.2016.09.014.

[40] G. Wang, C. Chen, and S. Yu, "Optimization and static output-feedback control for half-car active suspensions with constrained information," *J. Sound Vibrat.*, vol. 378, pp. 1–13, Sep. 2016, doi: 10.1016/j.jsv.2016.05.033.

[41] J. Mrazgua, R. Chaibi, E. H. Tissir, and M. Ouahi, "Static output feedback stabilization of T-S fuzzy active suspension systems," *J. Terramechanics*, vol. 97, pp. 19–27, Oct. 2021, doi: 10.1016/j.jterra.2021.05.001.

[42] M. Fleps-Dezasse, M. M. Ahmed, J. Brembeck, and F. Svaricek, "Experimental evaluation of linear parameter-varying semi-active suspension control," in *Proc. IEEE Conf. Control Appl. (CCA)*, Sep. 2016, pp. 77–84, doi: 10.1109/CCA.2016.7587825.

[43] Y. Qin, C. Xiang, Z. Wang, and M. Dong, "Road excitation classification for semi-active suspension system based on system response," *J. Vibrat. Control*, vol. 24, no. 13, pp. 2732–2748, Jul. 2018, doi: 10.1177/1077546317693432.

[44] M. M. Morato, M. Q. Nguyen, O. Sename, and L. Dugard, "Design of a fast real-time LPV model predictive control system for semi-active suspension control of a full vehicle," *J. Franklin Inst.*, vol. 356, no. 3, pp. 1196–1224, Feb. 2019, doi: 10.1016/j.jfranklin.2018.11.016.

[45] Y. Liu and L. Zuo, "Mixed skyhook and power-driven-damper: A new low-jerk semi-active suspension control based on power flow analysis," *J. Dyn. Syst., Meas., Control*, vol. 138, no. 8, Aug. 2016, Art. no. 081009, doi: 10.1115/1.4033073.

[46] A. Soliman and M. Kaldas, "Semi-active suspension systems from research to mass-market—A review," *J. Low Freq. Noise, Vibrat. Act. Control*, vol. 40, no. 2, pp. 1005–1023, Jun. 2021, doi: 10.1177/1461348419876392.

[47] A. P. A. da Silva and D. M. Falcão, "Fundamentals of genetic algorithms," in *Modern Heuristic Optimization Techniques*, K. Y. Lee and M. A. El-Sharkawi, Eds., 1st ed., Hoboken, NJ, USA: Wiley, 2008, pp. 25–42, ch. 2, doi: 10.1002/9780470225868.
[48] O. Bozorg-Haddad, M. Solgi, and H. A. Loáiciga, "Genetic algorithm," in *Meta-Heuristic and Evolutionary Algorithms for Engineering Optimization*, O. Bozorg-Haddad, M. Solgi, and H. A. Loáiciga, Eds. Hoboken, NJ, USA: Wiley, 2008, pp. 53–67, ch. 4, doi: 10.1002/9781119387053.
[49] N. Hansen, S. D. Müller, and P. Koumoutsakos, "Reducing the time complexity of the derandomized evolution strategy with covariance matrix adaptation (CMA-ES)," *Evol. Comput.*, vol. 11, no. 1, pp. 1–18, Mar. 2003, doi: 10.1162/106365603321828970.

YONGHWAN JEONG received the B.S. and Ph.D. degrees in mechanical engineering from Seoul National University, South Korea, in 2014 and 2020, respectively. From 2020 to 2021, he was a Senior Research Engineer with Hyundai Motor Company, South Korea. Since 2021, he has been an Assistant Professor with the Department of Mechanical and Automotive Engineering, Seoul National University of Science and Technology, South Korea. His research interests include sensor fusion with vehicular communication, risk assessment, driver intention inference with trajectory prediction, and motion planning and control of urban automated vehicle.

YOUNGIL SOHN received the B.S. and M.S. degrees in mechanical engineering from the Korea Advanced Institute of Science and Technology (KAIST), South Korea, in 1994 and 1996, respectively. From 1996 to 2012, he was a Principal Research Engineer with the Institute for Advanced Engineering (IAE), South Korea. From 2012 to 2021, he was a Senior Research Engineer with the Research and Development Center, Hyundai Motor Company, South Korea. Since 2021, he has been working as a Senior Research Engineer with the Institute of Advanced Technology Development (IATD), Hyundai Motor Company. His research interests include control software development for semi-active and active suspension for vehicle ride comfort, and artificial intelligent application for vehicle chassis control.

SEHYUN CHANG received the B.S. degree from Korea Aerospace University, South Korea, in 1996, the M.S. degree in aeronautical engineering from Seoul National University, South Korea, in 1998, and the Ph.D. degree in mechanical engineering from the University of Michigan, Ann Arbor, MI, USA, in 2007. Since 2007, he has been a Senior Research Engineer at the Research and Development Center, Hyundai Motor Company, South Korea. His research interests include vehicle dynamics, integrated chassis control, model predictive control, future mobility, and design optimization.

SEONGJIN YIM (Member, IEEE) received the B.S. degree in mechanical engineering from Yonsei University, South Korea, in 1995, and the M.S. and Ph.D. degrees in mechanical engineering from the Korea Advanced Institute of Science and Technology (KAIST), in 1997 and 2007, respectively.

From 2008 to 2010, he was a Postdoctoral Researcher with the BK21 School for Creative Engineering Design of Next Generation Mechanical and Aerospace Systems, Seoul National University. From 2011 to 2013, he was a Research Professor with the Advanced Institutes of Convergence Technology, Seoul National University. Since 2019, he has been an Associate Professor with the Department of Mechanical and Automotive Engineering, Seoul National University of Science and Technology, South Korea. His research interests include autonomous driving, integrated chassis control systems with V2V communication, cloud computing-based vehicle control, and active suspension control.